Journal of Geochemical Exploration 177 (2017) 45–60

Contents lists available at ScienceDirect

Journal of Geochemical Exploration

journal homepage: www.elsevier.com/locate/gexplo

Hydrothermal alteration of volcanic rocks in Seival Mine Cu–mineralization – Camaquã Basin – Brazil (part I): Chloritization process and geochemical dispersion in alteration halos

Eduardo Fontana [a,b,*], André S. Mexias [a], Christophe Renac [b], Lauro V.S. Nardi [a], Rodrigo W. Lopes [a,b], Aurélie Barats [b], Marcia E.B. Gomes [a]

[a] UFRGS – Universidade Federal do Rio Grande do Sul, Av. Bento Gonçalves 9500 – Agronomia, Porto Alegre, RS, Brazil
[b] Université Côte d'Azur, CNRS, OCA, IRD, Géoazur, 250 rue Albert Einstein, Sophia Antipolis 06560, Valbonne, France

ARTICLE INFO

Article history:
Received 26 June 2016
Revised 25 November 2016
Accepted 26 February 2017
Available online 2 March 2017

Keywords:
Geochemistry
Hydrothermal alteration
Chloritization process
C/S mixed–layers
Cu–sulfides

ABSTRACT

The Seival Mines are situated in the NE portion of the Lavras do Sul mining district, southernmost Brazil. They are hosted by volcanic and sub-volcanic rocks of Neoproterozoic age, which are part of the post–collisonal Camaquã Basin volcano–sedimentary sequence. The mineralization occurs in shoshonitic volcanic and sub–volcanic rocks of the Lavras do Sul Shoshonitic Association. They are of intermediate composition and exhibit widespread hydrothermal alteration. The mineralization occurs primarily in the form of bornite, chalcocite, covellite, pyrite, and in supergene phases as malachite. Mineral occurrence is always controlled by fractures. Ore is associated with chloritization processes, which produced smectite, chlorite/smectite and corrensite clay minerals and gangue of carbonate, mostly calcite, and barite. In this study field mapping and drill core sampling, petrography with optical microscopy and electron microscopy, X–ray diffraction for clay size fraction characterization and whole–rock geochemistry are used to understand the spatial distribution and relative chronology of hydrothermal alteration products of different lithology in the mineralized zones. The post–magmatic fluid activity and hydrothermal lower–temperature alteration that produced smectite ➔ chlorite/smectite ➔ chlorite and corrensite ➔ carbonate have changed the major, minor, trace and rare earth element (REE) contents. Lavas and sub-volcanic rocks contain Cu–Fe sulfides. In alteration halos, Cu–sulfides with supergene influence is related to circulation of late hydrothermal fluids. The pH variations and sulfide materials are related to dispersion metals around vertical structures.

1. Introduction

The Lavras do Sul mining district in Rio Grande do Sul, Brazil contains Pb, Zn, Au, Ag and Cu deposits associated with hydrothermal alteration that are hosted by Neoproterozoic volcano–sedimentary sequences and igneous intrusions (Nardi and Lima, 1988; Vieira and Soliani, 1989; Mexias et al., 1990; Mexias et al., 1991a, 1991b; Lima and Nardi, 1998a; Gastal and Lafon, 1998; Gastal, 1999; Bongiolo et al., 2007, 2008, 2011; Gastal et al., 2015). The hydrothermal alteration, metal distribution and consequent ore deposition by epithermal processes have previously been reported in the area. The high to low sulfidation mineral assemblages have been associated with a post–collisional magmatic–tectonic context (Mexias et al., 2007; Bongiolo et al., 2011; Müller et al., 2012; Lopes et al., 2014; Remus et al., 1997, 2000; Renac et al., 2014).

This project focuses on the Seival Mines which are situated in the NE portion of the Lavras do Sul city and hosted by volcanic rocks of the Hilário Formation (Ribeiro and Fantinel, 1978). These mines were the most important Cu–mines in the region during the first half of the twentieth century. Research on mineral exploration resulted in several regional scientific papers (Teixeira, 1937; Leinz, 1946; Leinz et al., 1947; Barbosa, 1958; Gavronski, 1963 and Robertson and Johnson, 1966). The mines comprise a set of small deposits with 0.6 to 2.5 wt% of Cu and up to 70 ppm of Ag (Reischl, 1978). These deposits are confined partly to Hilário Formation volcanic sequence and concentrated in areas without apparent continuity. The mineralization is mainly in the form of sulfides, bornite, chalcocite, covellite and supergene phases as malachite. It is controlled by fractures and faults oriented predominantly NE in extrusive and sub–volcanic rocks. Ore is associated with a

* Corresponding author at: UFRGS – Universidade Federal do Rio Grande do Sul, Av. Bento Gonçalves 9500 – Agronomia, Porto Alegre, RS, Brazil.
E-mail addresses: eduardo.fontana@ufrgs.br (E. Fontana), andre.mexias@ufrgs.br (A.S. Mexias), christophe.renac@unice.fr (C. Renac), lauro.nardi@ufrgs.br (L.V.S. Nardi), rodrigo.winck@ufrgs.br (R.W. Lopes), aurelie.barats@unice.fr (A. Barats), marcia.boscato@ufrgs.br (M.E.B. Gomes).

http://dx.doi.org/10.1016/j.gexplo.2017.02.004
0375-6742/

gangue of carbonate, barite and clays. The Cu–rich ore is generally disseminated or fills small cavities and fractures associated with argillic and propylitic alteration (Lopes et al., 2014).

Field descriptions, petrography, mineral and whole–rock chemistry were used in order to study the distribution of hydrothermal alteration products of different lithology in the mineralized zones of Seival Mine. The chronology of alteration events and their spatial distribution combined with whole–rock geochemistry contribute to understanding of the alteration sequence and its relationship with the Cu deposition in the Seival Mine.

2. Geological settings

The configuration of Brasiliano–Pan–African belts in West Gondwana and its relationship with the remaining cratons during the Neoproterozoic (880 to 550 Ma) is fundamental to understand the tectonic evolution of the southernmost Brazilian shield. The southernmost Brazilian shield is compartmented in four geotectonic units: (i) Taquarembó Block, composed of Archean rocks which were metamorphosed during the Paleoproterozoic; (ii) São Gabriel Arc, composed of Neoproterozoic rocks (900 to 700 Ma) comprising the intercalation of gneisses, amphibolites, granitoids and low–grade metamorphic rocks, (iii) Porongos Belt, composed of Paleoproterozoic metamorphic rocks of greenschist to amphibolite facies, reworked at the beginning of Ediacaran period (660 to 580 Ma) and covered by the volcano–sedimentary rocks from Camaquã Basin (640 to 450 Ma); and (iv) Pelotas Batholith, including mostly Neoproterozoic granitoids (630 to 550 Ma) and subordinate metamorphic rocks (Fig. 1–A). The details of the geodynamic evolution of tectonic blocks underlying the Camaquã Basin were previously described in several papers (e.g. Hallinan et al., 1993; Chemale et al., 1995; Saalmann et al., 2005; Hartmann et al., 2011; Saalmann et al., 2007, 2011).

The Camaquã Basin (Fig. 1–A) (Chemale, 2000; Paim et al., 2000; Wildner et al., 2002) located in the central part of the state of Rio Grande do Sul, southern Brazil, is composed of volcano–sedimentary sequences of Neoproterozoic age and contains the largest Cu, Pb, Zn and Ag deposits of this region, firstly described by Carvalho (1932). Camaquã Basin is a strike–slip basin formed in the final stage of the Brasiliano cycle (Wernick, 1978; Machado and Fragoso-Cesar, 1987; Brito Neves and Cordani, 1991). The stratigraphic evolution of Camaquã Basin has been discussed (Melcher and Mau, 1960; Goni et al., 1962; Robertson, 1966; Ribeiro and Fantinel, 1978; Fragoso-Cesar et al., 1985). The volcano–sedimentary basins of Camaquã Basin are related to a transcurrent system of deformation in a post–collisional context (Wildner et al., 1999, 2002), with collapsed tectonic blocks (Saalmann et al., 2011).

The Neoproterozoic sequences in the southernmost Brazilian shield occur in the SE, E and NE parts and consist of magmatic associations that show subalkaline medium to high–K, to shoshonitic, and sodic silica saturated alkaline affinities (Bitencourt and Nardi, 1993; Wildner et al., 2002; Sommer et al., 2006). The Hilário Formation (Ribeiro and Fantinel, 1978) is part of Lavras do Sul Shoshonitic Association, which contains the rocks of shoshonitic affinity, and includes the oldest volcanic rocks of Camaquã Basin sequence. Lima and Nardi (1998a) have related this shoshonitic volcanism to coeval monzonitic to quartz–monzonitic and lamprophyric hypabyssal magmatism. The hydrothermal alteration present in the eastern portion of the Lavras do Sul Shoshonitic Association, near the contact with the monzonitic to monzogranitic rocks (Mexias et al., 1991a,b) is associated with magmatic fluids (Lima and Nardi, 1998a) and with the generation of ore bodies (Au, Pb, Cu) (Fig. 1–B). U–Pb (Gastal et al., 2005; Liz et al., 2009) and Ar–Ar ages (Janikian et al., 2008) from the Lavras do Sul Shoshonitic Association and Hilário Formation vary from 583 to 601 Ma (Gastal et al., 2005; Liz et al., 2009), which is considered as the age range of shoshonitic magmatism in the Camaquã sequence. In the eastern portion of Lavras do Sul Shoshonitic Association, hydrothermal and magmatic processes generated disseminated Cu–ore, described as the Seival Mines. In the Seival Mines area, the N–NE ruptil structures result largely on the reactivation of the regional shear zones. The main regional structures that affected the Hilário Formation are part of a NW fault system, correlated with the Ibaré Shear Zone (Paim et al., 2000 and Borba et al., 2008). According to Porcher and Lopes (2000), this zone of strike–slip faults of Proterozoic age and intermediate crustal level, shows evidence of several reactivations during the Phanerozoic and has controlled the deposition of the sediments of Paraná Basin.

3. Materials and methods

Eleven hand specimens from surface outcrops of background volcanic rocks and ores were collected from Seival Mine region. They consist of samples from subvolcanic, lava and pyroclastic rocks, with variable hydrothermal alteration. This sampling was complemented by thirteen whole–rock fragments collected from four drill cores that intersect the volcanic sequences of SM. This sampling covered two regions Location 1 (L–1) and location 2 (L–2) (Fig. 2–A and B). On location 1, in the north portion of the area, the samples were collected from the surface (1–9, Fig. 2–A). In location 2 (center of the area) samples were collected in surface (1, 2) and drill cores (1–30, Fig. 2–C). Petrographic, mineralogical identification and modal quantification were obtained from optical microscopy and Scanning Electron Microscopy (SEM) and Energy Dispersive X–ray Spectroscopy (EDS), Zeiss EVO LS15, 20 kV, 2.5 nA with X–Max Oxford EDS detector, IAEA Monaco and Jeol 6610–LV – EDS, LGI–UFRGS. The observation and preliminary work of fluid inclusion assemblages was observed by optical microscopy and crushing to identify of CO_2 and CH_4 liquid. The alteration mineralogy was realized by X–ray diffraction (XRD; BRUKER AXS SIEMENS Model D5000 Cu $K\alpha_{1+2}$, 40 kV and 25 mA). Clay–size fractions were separated from powdered samples settled to recover <4 μm. Crystallographic characterization were performed and determined relative proportions in clay–rich materials (<4 μm) using air–dried oriented preparation, glycolated solvatation and heated at 550 °C for 2 h. Clay mineral content was estimated using the NEWMOD *software* (Reynolds, 1985). Whole–rock samples as well as hydrothermal alteration products were collected and pulverized. Whole–rock samples were first fused and analyzed for major and trace elements in the Activation Laboratories Ltd., Ontario, Canada, by Inductively Coupled Plasma Atomic Emission Spectrometry (ICP–AES) and Inductively Coupled Plasma Mass Spectrometry (ICP–MS). In strategic samples, it was carried out with technical breakdown and micro sampling with diamond drill and split with binocular magnifying glass for whole–rock analysis. Contents of minor, trace and REE elements were measured after acid digestion dissolution of powdered rocks with HNO_3 2 cm^3 15 N, HF 1 cm^3 20 N ultrapure both. All digested solutions were analyzed by ICP–MS (Elan DRCII, Perkin Elmer) at the University of Nice Sophia–Antipolis. Detection limits are below 50 $ng \cdot L^{-1}$.

4. Results

4.1. Lithologies and textures of volcanic rocks

The Seival Mine Cu ore is hosted by pyroclastic, effusive and subvolcanic rocks. The pyroclastite are dominantly lapilli–tuff with less amounts of tuff–breccia (Fig. 3–A). The upper sequence (L2–1 and 2; DH–2 and 3) consists of trachytic lava flows with vesicular textures (Fig. 3–B). The subvolcanic rocks enveloped by lapilli–tuff and lavas occur parallel to the volcanic lava flows with predominant NE/NW directions (Fig. 2–A, B and C). Subvolcanic rocks show andesite–type porphyritic texture.

In the Seival Mines area, drill holes sampled >300 m of pyroclastic and lava flows (L2 area) and a few meters of subvolcanic rocks (DH3 and 4, Fig. 2–C). Feldspar phenocrysts occur parallel to the lapilli–tuff – subvolcanic rocks contact where the matrix is altered to materials of predominantly white colours (DH4–24) (Fig. 2–C). The Seival Mines effusive and subvolcanic rocks also contain calcite disseminated or

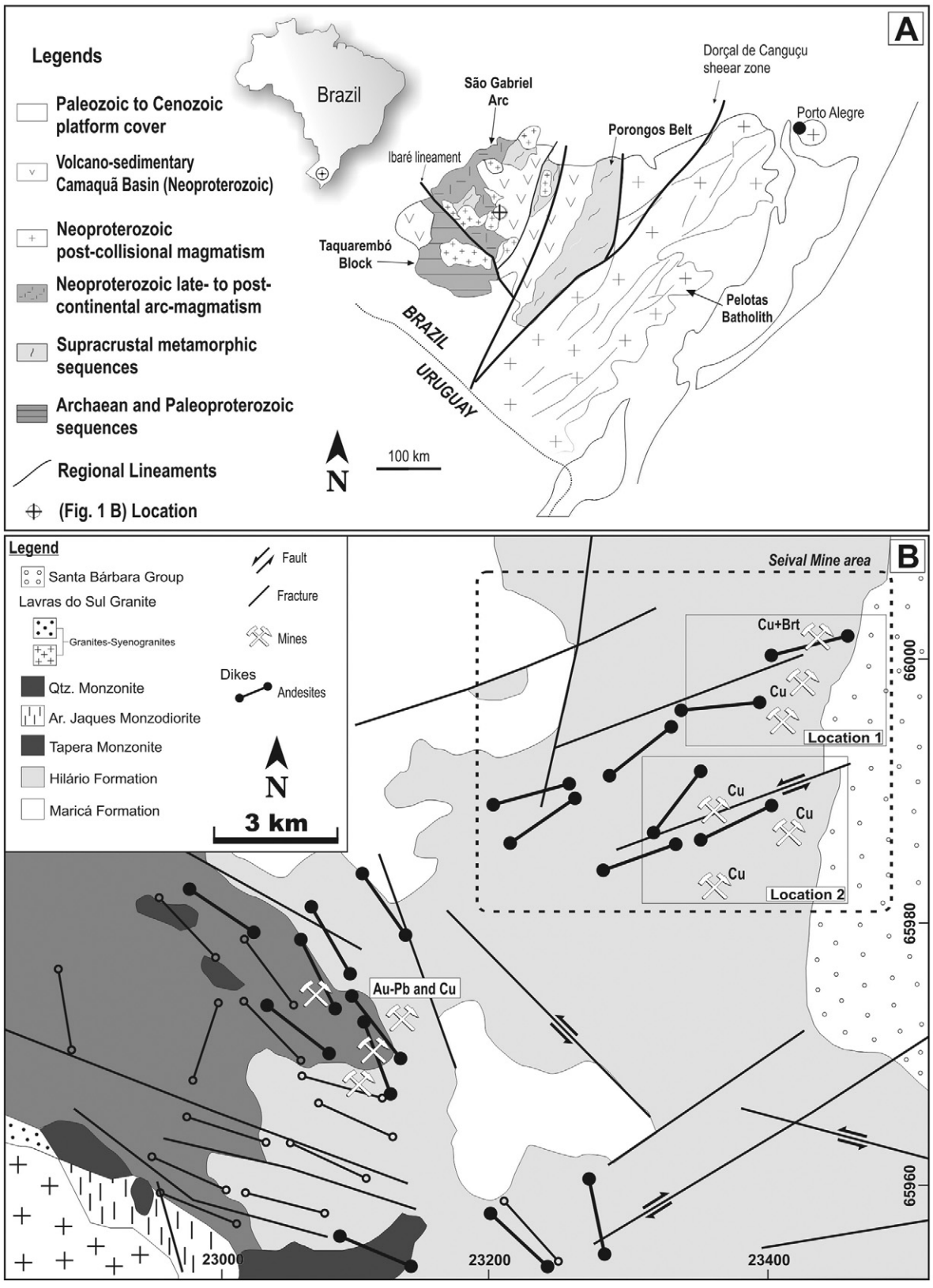

Fig. 1. Tectonic setting of Neoproterozoic post–collisional magmatism and volcanic rocks of Hilário Formation: A) Geotectonic units of southernmost Brazilian shield; B) Simplified geological map of Lavras do Sul plutonic and volcanic rocks. The construction of this map after Reischl, 1978; Lima and Nardi, 1998a; Gastal et al., 2005; Wildner et al., 2008; Liz et al., 2009; Bongiolo et al., 2011; Janikian et al., 2012; Lopes et al., 2014 and Gastal et al., 2015.

filling vesicles and veins (Fig. 3–A and B). Parts of lava flows enriched in vesicles fulfilled by calcite (Cal–1, Fig. 3–B) are crosscut by calcite–rich veins further described as Cal–2 and Cal–3. Cal–2 contains *c.* 1.2 at.% of Fe, and Cal–3 *c.* 1.2 at.% of Mn. Quartz, sometimes as euhedral grains, occurs filling vesicles and veinlets that cut Cal–2 and Cal–1. Cal–3 veins contain fragments of host–rocks, minor sulfide grains and barite.

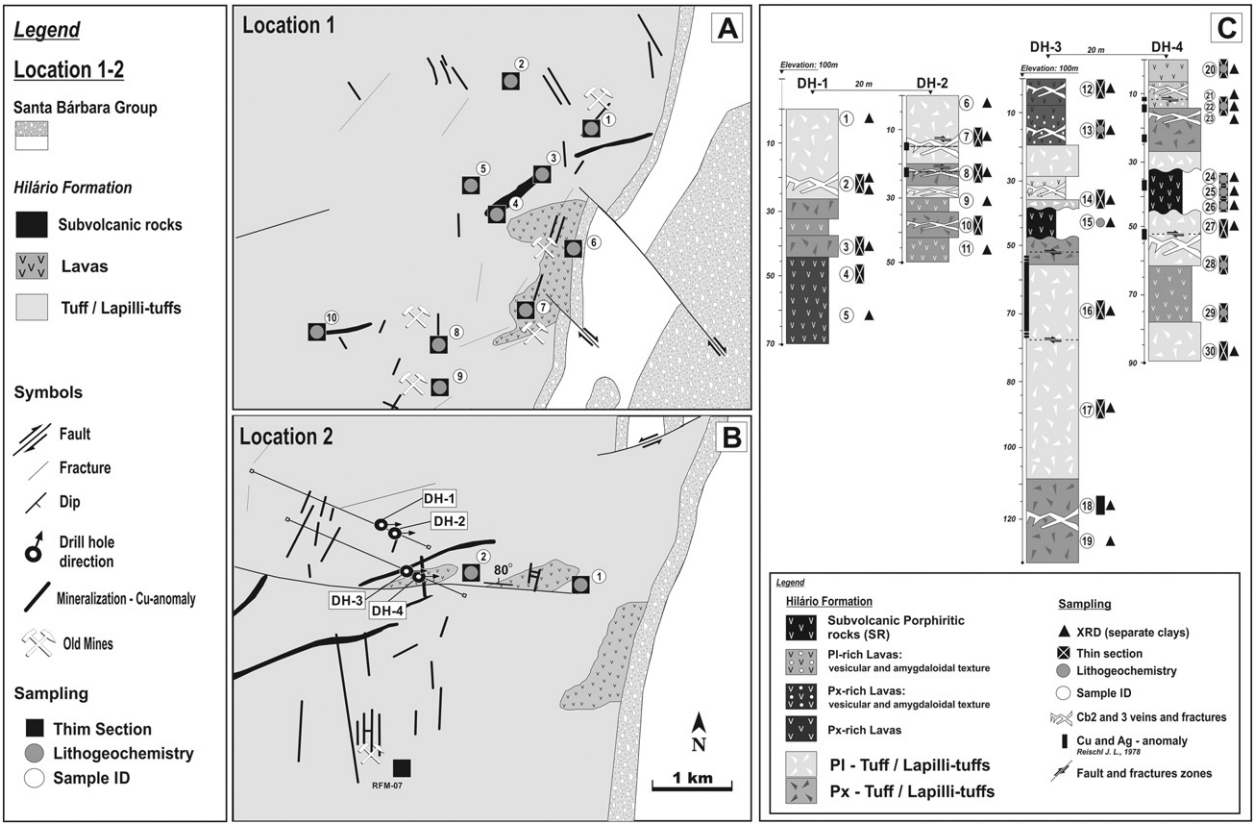

Fig. 2. A and B) L1 and L2: extrusive rock samples (pyroclastic and lavas) from L1/1, 2, 5–8 and L2/1, 2; porphyritic andesite in L1/2, 3 and 9; C) Simplified stratigraphic column is presented with sedimentological settings. Adapted from: Reischl, 1978 and Lopes et al., 2014. Extrusive rock samples (pyroclastic and lavas) from DH–1 to 4: 1–14; 16–23; 26–30 and porphyritic andesite in DH/3 and 4: 15; 24–26.

In the mining area L1–1 (Fig. 2–C), fractured rocks are replaced by green–coloured materials composed of malachite associated with Sr–rich barite (XRD) and hematite.

4.2. Petrography and mineralogy

The lapilli tuff show an altered matrix containing fragments of andesine–oligoclase and augite, as well as clasts of andesitic rocks. The altered LT matrix is a mixture of clay minerals and carbonate (Fig. 4–A and B). Fe–Ti oxides, anhedral chalcocite and bornite occur in Cal–2, Cal–3, and barite veins.

The lavas have trachytic texture with phenocrysts of Pl and Px (Fig. 4–C and D). The altered matrix contains relictual Pl, Px, glass and microliths which are replaced by quartz, clays, carbonate with minor epidote + titanite, iron oxides, euhedral pyrite and vesicles filled by green clays and quartz (Fig. 4–C) or carbonate (Cal–1; Fig. 4–D). In the L rocks, millimetric fractures are filled by carbonate previously described as Cal–2 and Cal–3. Carbonates (Cal–1 to 3) contain primary and secondary aqueous fluid inclusions with H_2O–CO_2 liquid in Cal–3 crystals.

The subvolcanic rocks collected in drill–holes (DH–3; DH–4, Fig. 4, E and F) have centimeter–sized phenocrysts of Pl and smaller Px. In the matrix and phenocrysts, clays fill vesicles and the Pl crystals. Thin section studies show phenocrysts of plagioclase and pyroxene (Fig. 4–E) in a matrix composed of oligoclase–andesine microliths (Fig. 4–F). Plagioclases, particularly the phenocrysts, are transformed to albite–epidote + titanite–"sericite"–white to green clays and carbonates.

4.2.1. Alteration mineral assemblages in volcanic rocks

Alteration mineral recognized by petrographic observation, SEM–EDS and powder XRD analyses are albite associated with white to dark green clay minerals, disseminated epidote + titanite, quartz, calcite and oxides. SEM–EDS observations revealed that colour and habits related to vesicle, pervasive alteration and veins are associated with relative changes in Al, Fe and Mg contents. X–ray diffractometry shows that clay–rich materials (<4 μm) are smectite, irregular chlorite/smectite (C/S) mixed–layers or corrensite (C/S regular mixed–layer) and chlorite (Fig. 5). The smectite and C/S were dominantly observed in lavas and lapilli–tuff rocks. In lavas smectite–rich is dominant and appears pleochroic ranging from orange to brown due to the fibrous habit of crystals (Fig. 6–C and D). XRD patterns indicate 90 to 100% smectite (Beaufort and Meunier, 1994) with ~10% of chlorite (Reynolds, 1985; EG patterns in Fig. 5–A and B) and semi–quantitative chemical analyses (SEM–EDS) suggest an Al–rich saponite with higher Mg content than Fe and minor Ca and Na. The oriented XRD patterns indicate that smectite have different state of hydratation related to the Na–Ca contents in the interlayer.

In lavas and lapilli–tuff, C/S fill the matrix porosity or cavities and S appears only in amygdal cavities (Fig. 6–C, E and F) and C/S irregular (dark green) is dominant in lapilli–tuff materials appear amygdaloidal cavities, fractures and the matrix porosity (SEM–EDS). The XRD patterns (AD and EG; Fig. 5–C) indicate irregular C/S mixed–layer with 30% chlorite and 70% smectite. These irregular C/S mixed layer contain higher or lower Mg–Fe contents and lower Ca content with minor K and Na contents than smectite previously described.

A light green clay mineral was recognized in all extrusive and subvolcanic rocks. In lapilli–tuff, this light green clay mineral is minor compare to dark green associated with calcite (Cal–2 and Cal–3) and hematite. The light green particles are Fe–rich clays with less or more Mg, and minor Na contents relative to Ca. (Fig. 6–G and H). XRD identified corrensite (Fig. 5–D) with 50% trioctahedral chlorite with 50% trioctahedral smectite (reference therein).

With XRD analyses, chlorite was recognized in the center of fracture associated with high Cu anomalies or replacing magmatic pyroxenes and feldspars in extrusive rocks (L and LT: L1–1, 7 and 8 in Fig. 2). Augite phenocrysts were replaced by Fe–rich chlorite (SEM–EDS) and typical

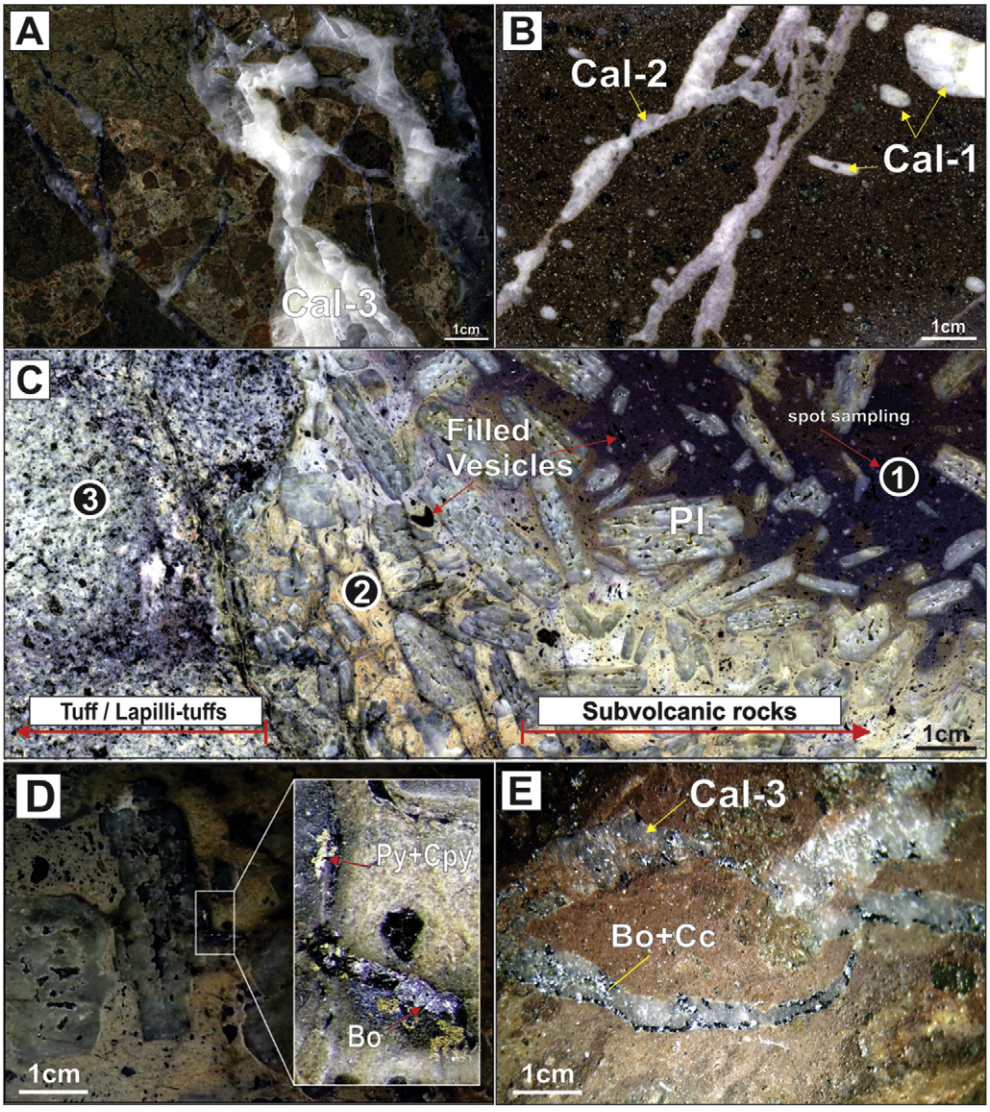

Fig. 3. Hand samples of different types studied in this work: A) drill hole section of the lapilli–tuff hand sample, DH1–2); B) drill hole section of lava sample containing hydraulic breccia with fractures and vesicles filled by carbonate (DH4–21); C) drill hole section of hand sample contact between lapilli–tuff and subvolcanic rock, DH–4–24; D) hand sample of subvolcanic rock, DH4–24; E) hand sample of lapilli–tuff with veins L1–8. (Cal–1, 2 and 3 = calcite; Py = pyrite; Bo = bornite; Cpy = chalcopyrite; Cc = chalcocite; "spot sampling" (*REE patterns* – Fig. 9).

XRD patterns show d_{001} at 14.2 Å and d_{002} = 7.3 Å. In the meantime, Na and Ca feldspars are altered into chlorite.

4.2.2. Cu–Fe–S sulfides and oxides

Petrographic, SEM/EDS patterns show different sulfides in the different Seival Mines lithologies. The bornite (Cu_5FeS_4) and chalcocite (Cu_2S) with later covellite (CuS) are dominant in lapilli–tuff and lavas inside faults and fractures. Hexagonal chalcocite is disseminated in micro fractures and porosity in the matrix of clast and lapillis associated with corrensite, hematite and ilmenite (Fig. 7–A and B); whereas in andesitic lavas, the pyrite ($CuFeS_2$) are dominant and minor bornite + chalcocite (Cu_2S) (Fig. 7–C and D). The sulfide assemblages are recognized similar to previous description (Reischl, 1978; Lopes et al., 2014), consisting in pyrite + chalcopyrite, bornite + chalcopyrite and some covellite (CuS) (Fig. 7–E and F) with scarce occurrences of native silver (Ag) with calcite and barite.

5. Geochemistry

Major element contents of SM samples with relatively low LOI (Loss on Ignition) values (this work and Lopes et al., 2014), plotted in Total Alkali Silica (TAS), Nb/Y vs. Ti/Zr (Pearce, 1996), and, *R1–R2* diagrams (De La Roche et al., 1980) are similar to those of Lavras do Sul Shoshonitic Association (Lima and Nardi, 1998b; Liz et al., 2009), although the subvolcanic rocks show slightly more alkaline compositions, consistent with more evolved sources. Trachytic and basaltic compositions with $K_2O > Na_2O$ are predominant, classifying the studied samples as potassic or shoshonitic, according to Le Maitre et al. (2005). Hydrothermal alteration, indicated mostly by higher LOI values, strongly increases CaO and C_{total} contents related to calcite as observed in veins and vesicles. Lavas and lapilli tuffs have Na–rich plagioclase. LOI values in subvolcanic rocks are lower, 2 to 5 wt%, than in effusive and pyroclastic rocks which show 6 to 10 wt%. CaO and C_{total} contents show positive correlation with LOI, SiO_2, Al_2O_3, whilst Na_2O contents decreases (Fig. 8).

The Sr contents are high, particularly in equigranular subvolcanic rocks and lapillit–tuffs (>800 ppm), but decrease in subvolcanic rocks and in hydrothermally altered samples. The Cu, Au, Ag, S and As concentrations show increased contents in the porphyritic lava and can reach high values in some samples with higher LOI. The Zn contents have higher values in the porphyritic lava, but decrease in samples with high LOI. The Nb and Y values are high in altered lapilli–tuff rocks compared to less altered smectite–rich lavas. The REE patterns of

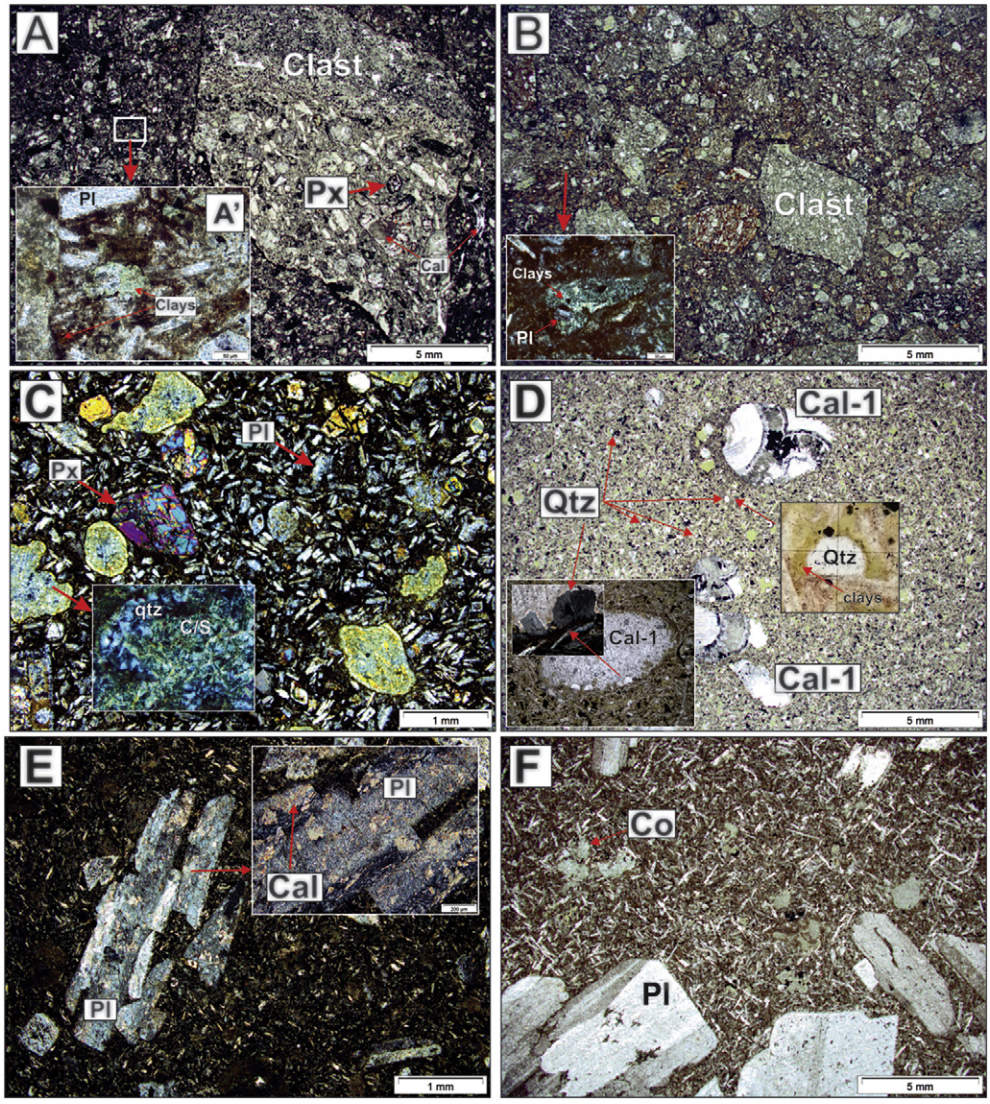

Fig. 4. Photomicrographs of thin sections obtained from samples of drill holes – Location 1 and 2: A) DH2/8 sample location lapilli–tuff containing altered green clast Px–rich; B) lapilli–tuff DH/27 sample location containing altered clasts; C) DH3/13 sample location extrusive rocks (lava flow) sample, having Px and Pl with vesicles filled by clays; D) DH4/25 sample location extrusive rocks (lava flow) sample carbonate filling vesicles in the matrix; E) Subvolcanic rocks L1/10 sample location containing plagioclase with calcite; F) subvolcanic rocks DH4/25 sample location with plagioclase altered to epidote + corrensite and illite. Cb1 = carbonate 1; Pl = plagioclase; Px = pyroxene; Qtz = quartz; Co = corrensite.

subvolcanic rocks, lavas and lapilli–tuff samples (Fig. 9) are similar to those reported by Lima and Nardi (1998b) in the Lavras do Sul Shoshonitic Association, and Lopes et al. (2014) in the Seival Mines area. Subvolcanic rocks have the highest ΣREE (total content of REE) values ranging from 193 to 240 ppm and in the lavas and lapilli–tuffs rocks ΣREE values range from 130 to 230 ppm. Their chondrite normalized patterns show LREE enrichment in relation to Heavy–REE with the values of La/Yb in subvolcanic rocks = 40 and in lavas and lapilli–tuffs = 30 in average. Less altered equigranular subvolcanic rocks show the highest concentrations of REE elements and slight negative Eu anomalies. Considering the variation of LOI, the REE behave like the high field strength elements (Heavy–REE), and tend to decrease when the LOI increase.

6. Discussion

6.1. Petrogenesis of volcanic material in the Seival area

The field studies, whole–rock geochemistry, petrographic and mineralogical observations show hydrothermal alteration, either related to post–lava deposition supergene alteration and to younger magmatic intrusions, both controlled by fractures (Fig. 10). The Lavras do Sul Granite Complex, part of the Lavras do Sul Shoshonitic Association (Lima, 1995; Nardi and Lima, 1985; Lima and Nardi, 1998a) shows a thin zone of contact metamorphism with the Hilário Formation (Mexias et al., 2005 – Volta Grande area and Bongiolo et al., 2011). Previous studies in the altered Lavras do Sul Shoshonitic Association highlighted the formation of episyenites in the granitic rocks (Mexias et al., 1990; Mexias et al., 2005) and, potassic, propylitic, phyllic to argillic alterations in granitic, volcanic and subvolcanic rocks of the Lavras do Sul Shoshonitic Association (Bongiolo et al., 2011) representing post–magmatic to the hypabyssal hydrothermal fluids in geothermal system. The Seival Mine area is located *c.* of 10 km from these previously studied areas, and consists of intermediate pyroclastic and lava flows (lavas and lapilli–tuff rocks) and intermediate sub–volcanic bodies correlated to monzonite intrusions described by Gastal et al. (2005) and Liz et al. (2009). Whole–rock geochemistry of extrusive and sub–volcanic rocks shows a prominent increase of Ca and LOI contents in hydrothermally altered samples. A preliminary geochemical interpretation indicates that magmas were derived from a potassic trachy–andesite composition with a shoshonitic affinity similar to Lavras do Sul Shoshonitic Association compositions (reference therein).

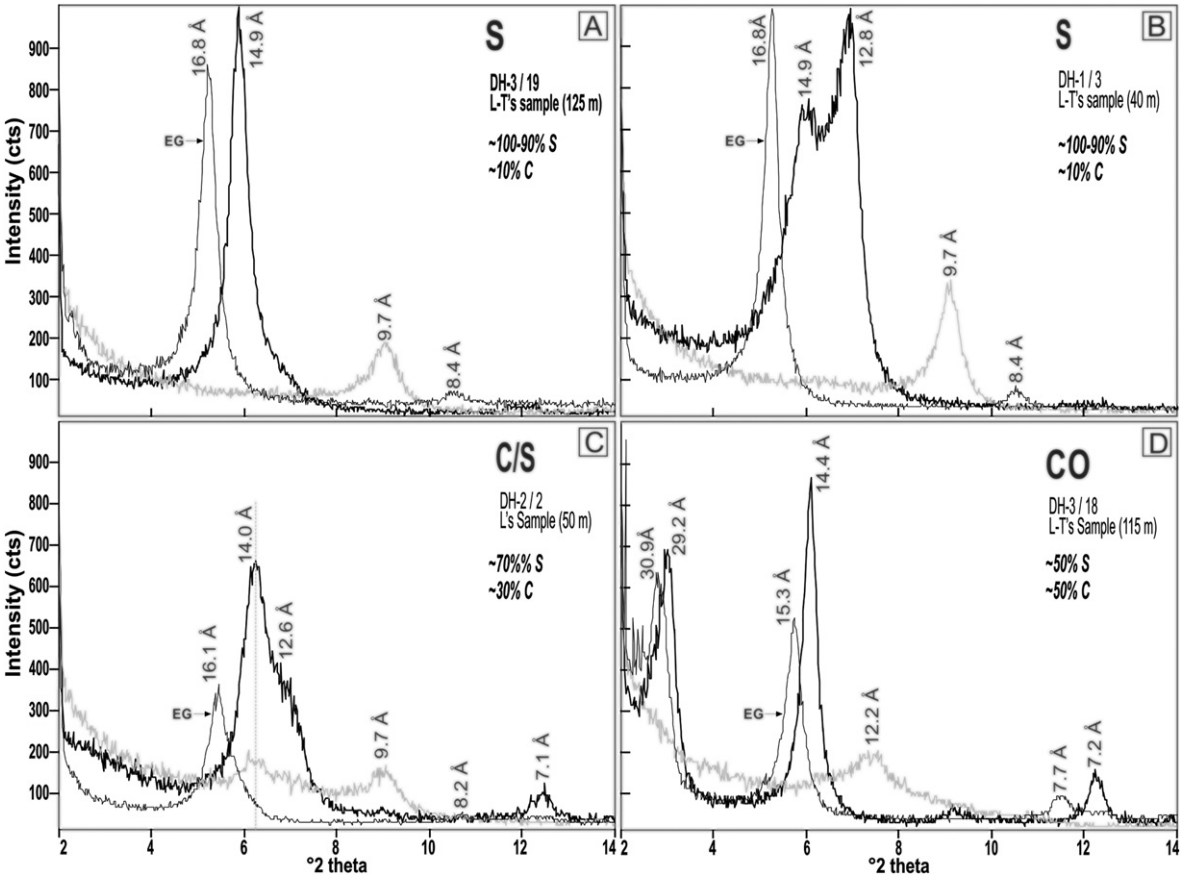

Fig. 5. XRD patterns of <4 μm clay size fraction, air dried (AD) = black line, after ethylene glycol solvation (EG) = gray and heating treatment (HT) = light gray.

The Lavras do Sul Shoshonitic Association andesite average composition (non-altered rocks) were compared with the lava with the lowest LOI (L1–3, Table 1). The C.I.P.W. (Cross et al., 1902; Johannsen, 1931 and Barth, 1955) normative contents of non-altered rocks and Seival Mine lavas with the lowest LOI, were compared, both show normative albite–anorthite–hypersthene with augite in the former and corindum in the Seival Mine lavas (L1–3). The normative albite–orthoclase and corindum in altered andesitic lava suggest either albitization or potassic alteration (Boles, 1982; Lee and Parsons, 1997; Hövelmann et al., 2010). In the most altered samples (LOI > 6%; Table 1) in agreement with mineralogical observation, normative calculations of alteration were estimated using major elements (Table 1) distributed in alteration end–members quartz, albite, orthoclase, oxides, apatite, carbonates and clay minerals (Kackstaetter, 2014). Petrographic data show that alteration in SM is dominated by albitization of plagioclase, deposition of calcite (Cal–1, Cal–2 and Cal–3) and formation of clay minerals. The XRD patterns and SEM–EDS identified K–feldspar, illite (DH4–24, 25 and DH3–15), smectite (S–rich irregular C/S), chlorite/smectite (chlorite–rich C/S), chlorite and corrensite. Consequently, the normative calculation of alteration products was modified to calculate proportions of illite, chlorite (chamosite) and smectite (saponite) further used as equivalent S, C/S, chlorite and corrensite proportions. The calculation of most altered rocks failed in a number of analyses by lack of Ca, Mg, Fe, and LOI or CO_2, interpreted as caused by presence of relictual pyroxene observed in thin sections of fresh and altered rocks (Table 1, subvolcanic rocks: L1–7, L1–3; lavas + lapilli–tuff: DH1–10). Consequently, for this normative calculation, samples with pyroxene observed in thin sections and 5 samples with LOI > 6% were discarded.

The normative calculation has distributed K in orthoclase and illite, Ca, Fe, Mg between carbonates and clays and, Na between albite and mainly in smectite (saponite). Five compositions over eight, with LOI higher than 6%, completed the calculations for 98% of the whole–rock composition. Calculations indicate dominant albite and clays, in similar proportions, for 2/3 of the alteration (26 to 44% of clays) quartz, calcite and oxide completing the mineralogy. The chamosite represents the largest component of clays (11 to 20 weight %, wt%) with smaller proportion of saponite (4 to 7 wt%) with 70 to 75% of chamosite in a chamosite + saponite mixed layer. The dominant proportion of 'calculated chamosite' is in agreement with clay mineral proportions observed in XRD patterns (chlorite > corrensite: L1–1, L1–4, L1–5) associated with minor proportions of illite and K–feldspar (L1–1). These calculations with dominant chamosite and no K–feldspar partially agree with a large number of XRD identification (L1–8, DH1–2). The calculations and observation that mismatches suggest the occurrence of different types of smectite and chlorite. Even after adjusting the normalization using corrensite and saponite end–members, calculation still overestimates the chlorite proportions, suggesting the occurrence of Al–rich chlorite rather than Mg–Fe one. Calculated carbonates, as calcite (Ca and CO_2), represent 8 to 19 wt% (DH2–1) in agreement with petrographic observation of Cal–2 and Cal–3 calcite–rich veins and disseminated carbonate in the matrix. Adjusting clay mineral end members (chamosite ➔ corrensite) does not modify calcite proportions.

6.2. REE signatures of the less and more altered volcanic rocks

Most lavas of the Seival Mine area have magmatic chemistry overprinted with hydrothermal alteration (calcite and clay minerals). Therefore, concentrations of major, minor and trace elements are modified such as Sr changes related to albitization or calcite contents. Consequently, geochemical source of magmatic material was rather studied using the REE patterns of less altered subvolcanic rocks with LOI < 2% and conserved pyroxenes. Such rocks have variable ΣREE contents with Light–REE enrichment and Eu negative anomaly (DH4–1 Eu_N, $Eu/Eu^* = 0.6$; Table 1; Fig. 9–A). These signatures are related to dominant proportions of albite (SEM observation) as phenocrysts or microliths

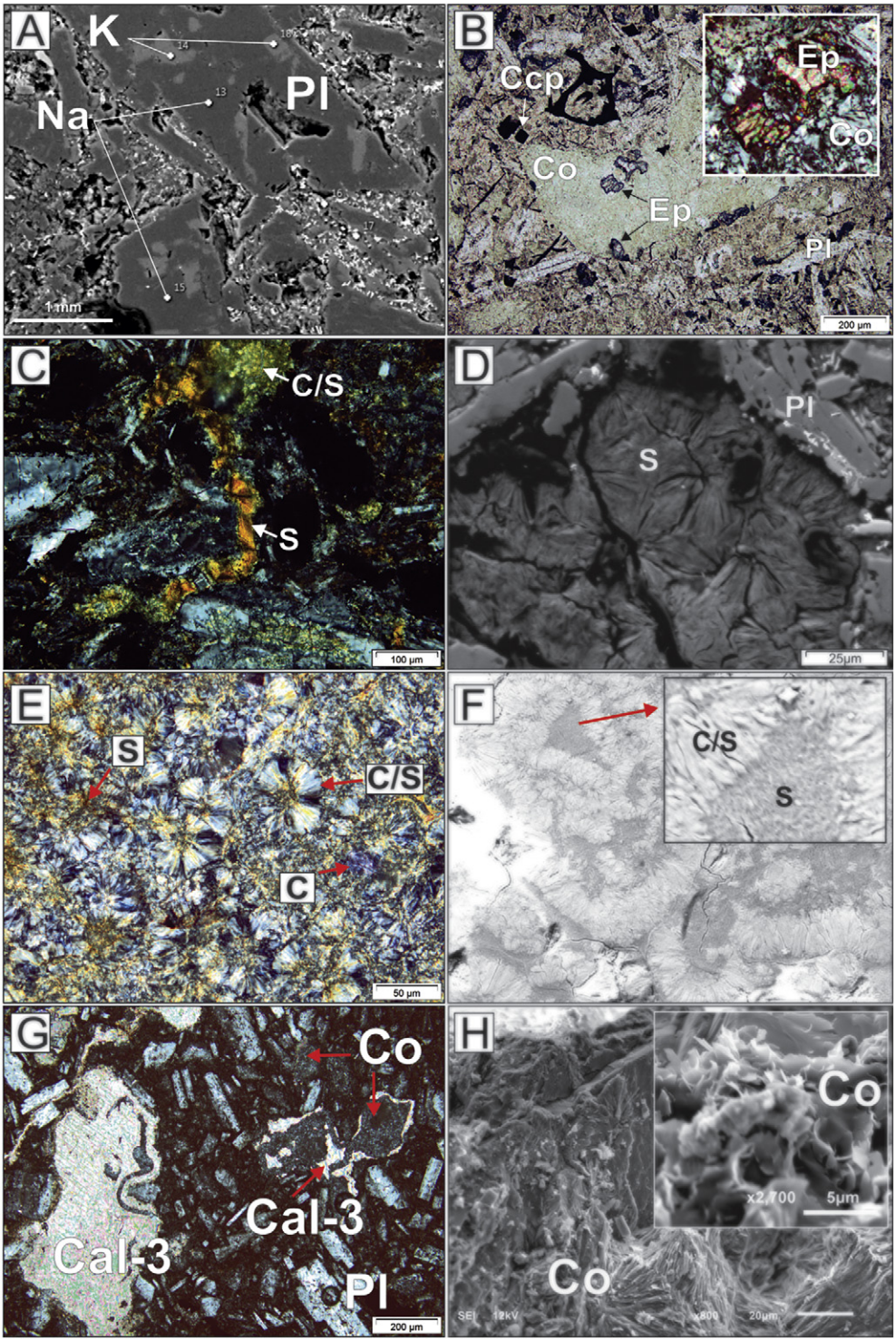

Fig. 6. Photomicrographs of Seival Mine rocks and SEM – EDS images with semi quantitative chemical results: A) SEM image of lava (DH4–21) containing K–altered in albite–rich Pl; B) photography of subvolcanic rock sample (DH4–25) containing epidote and Co filling vesicles; C) photography of lavas sample containing smectite and minor C/S (DH4–30); D) SEM image with detail of smectite (saponite) amygdaloidal cavities located in the matrix of lavas (DH4–30); E) photography of lavas sample containing smectite and C/S filling vesicle (DH4–30); F) SEM image with detail of smectite and C/S filling vesicle (DH4–30); G) photography of lavas sample containing corrensite with calcite filling vesicles in the matrix of lavas (DH4–21); H) SEM image of corrensite filling vesicles (DH4–21). Pl = plagioclase; C = chlorite; Cal = calcite; S = smectite; C/S = chlorite and smectite mixed layers.

in the matrix. In order to follow REE changes related to subvolcanic rocks (point 1 and 2) and lapilli–tuff (point 3) interaction, a section of four rock samples were analyzed (Fig. 3–C). Petrography and mineralogy (SEM–EDS, XRD) indicate with the occurrence of microlithic albite with dominant and disseminated corrensite and calcite (point 1). The subvolcanic rock border contains vesicles filled with corrensite and albite microliths (point 2). The lapilli–tuff sample contains albite microliths with dominant S–rich irregular C/S (point 3 and 4). Therefore, the strong modifications of REE patterns record albitized subvolcanic rocks with corrensite (subvolcanic rocks) and albitized lapilli–tuff with S–rich irregular C/S. The occurrence of albite in all matrices suggests that strong modifications of ΣREE concentrations with more negative Eu DH4–4 Eu_N, $Eu/Eu^* = 0.9$, Gd and Yb anomalies are related to S–rich irregular C/S and corrensite precipitations. Moreover,

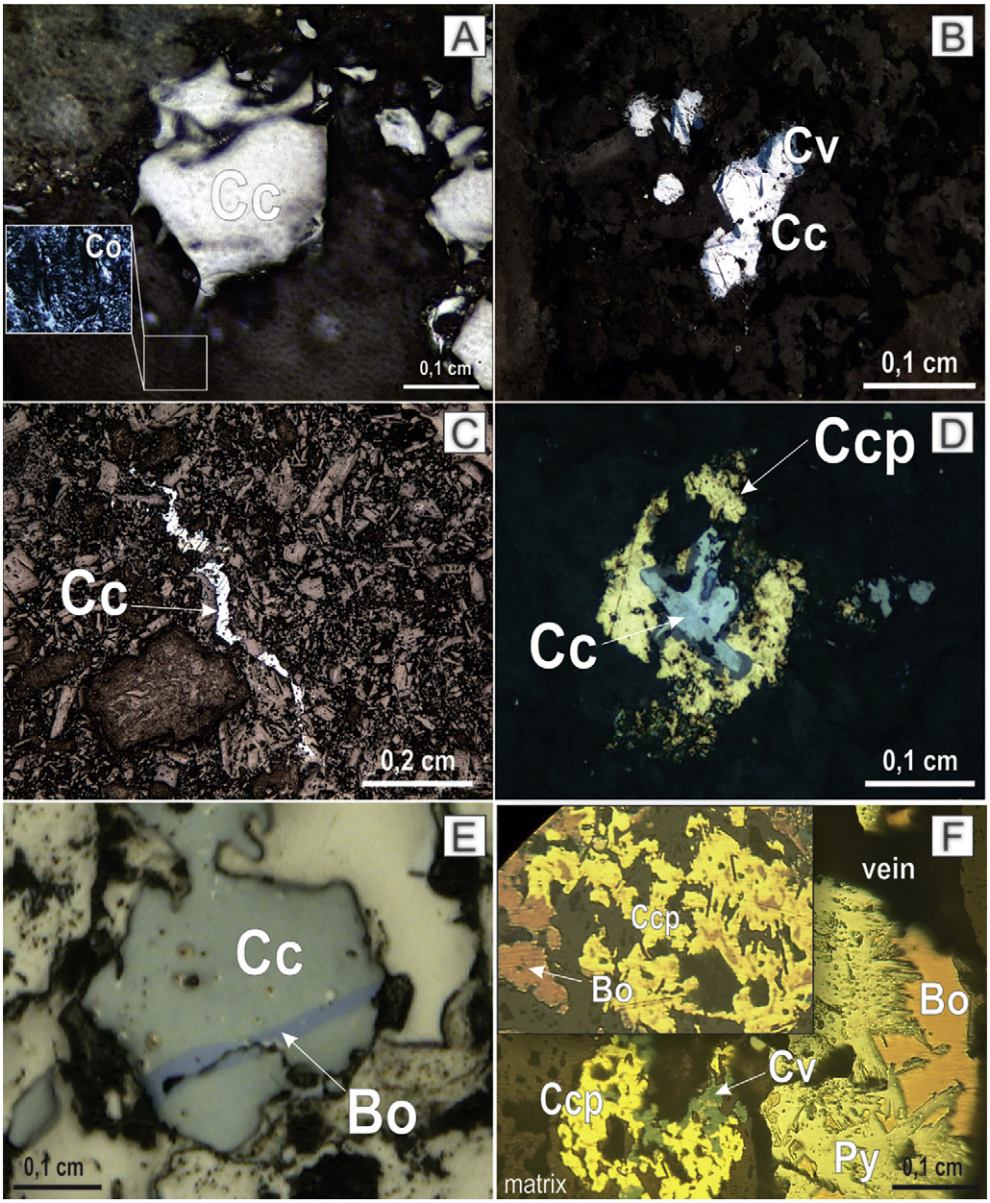

Fig. 7. Sulfides in the rocks of Seival Mine: A) hexagonal form Cc associated with Co (L1–6); B) Association between Cc + Cv – lapilli–tuff in DH–7 sample; C) Cc vein in a matrix of lava sample from drill core (DH–2); D) Ccp + chalcocite coronitic reaction in DH–2; E) Cc + bo layers of reaction (L1–3); F) assemblage of bo + ccp in D1 (left and top) and assemblages between py + bo forming a thin sulfide veins (DH–4). Py = pyrite; Ccp = chalcopyrite; Bo = bornite; Cc = chalcocite; Cv = covelitte; Co = corrensite.

preserved lapilli tuff textures suggest that chemical changes as dominantly associated with volcanic glass. Consequently, REE and the Eu, Yb negative anomalies would represent to some extent the glass composition and accessory minerals. REE concentration as related to the addition of H_2O and Fe–Mg precipitating corrensite, this interpretation would have to be check by mass balance calculation.

6.3. Relative chronology and chloritization processes in the Seival Mine

Field and drill cores allow schematic sequence of clay precipitation with a petrographic relative chronology to be observed (Fig. 10). Actual observation shows small proportion of disseminated smectite in lavas and lapilli–tuff replacing glass and filling vugs. The temperature of smectite phase formation (considered in this work as post–volcanic circulation fluids origin) is <100 °C (Farmer et al., 1991, 1994; Vogels et al., 1995). The transformation of C/S from volcanic smectite materials is previously suggested to occur in response to an increase of temperature (Bettison and Schiffman, 1988). A variation of S proportion with <20% chlorite is also supposed to occur with increasing temperature in hydrothermal environments (Inoue et al., 1984; Inoue, 1987; Inoue and Utada, 1991). However, the temperature could play a secondary role in C/S formation and can be controlled by different water/rock ratio (Bettison-Varga and Mackinnon, 1997). Nevertheless, the C/S formation suggests a temperature of precipitation lower than chlorite/epidote + titanite temperature, with an increasing Ca and Mg activity in hydrous fluids (Meunier, 2005). Kameda et al. (2011) estimated C/S formation in faults by frictional heating. This temperature domain between 185 and 260 °C. These S–rich irregular C/S seems to grow from smectite (SEM–EDS). The observation of lavas, lapilli–tuff contact with subvolcanic rocks show a chilled margins indicating intrusive materials in lavas and lapilli–tuff. In the center of the bodies this intrusive subvolcanic rocks is pervasively altered to corrensite. Moreover, minor proportion of corrensite associated with calcite (Cal–2 and 3) occurs in lapilli–tuff associated with small veins in fault zones. Crushing tests were performed in these calcite veins only on the Cal–3 which have $CO_{2liquid}$ into the bi–phasic fluid inclusions. Bubble expansion indicates

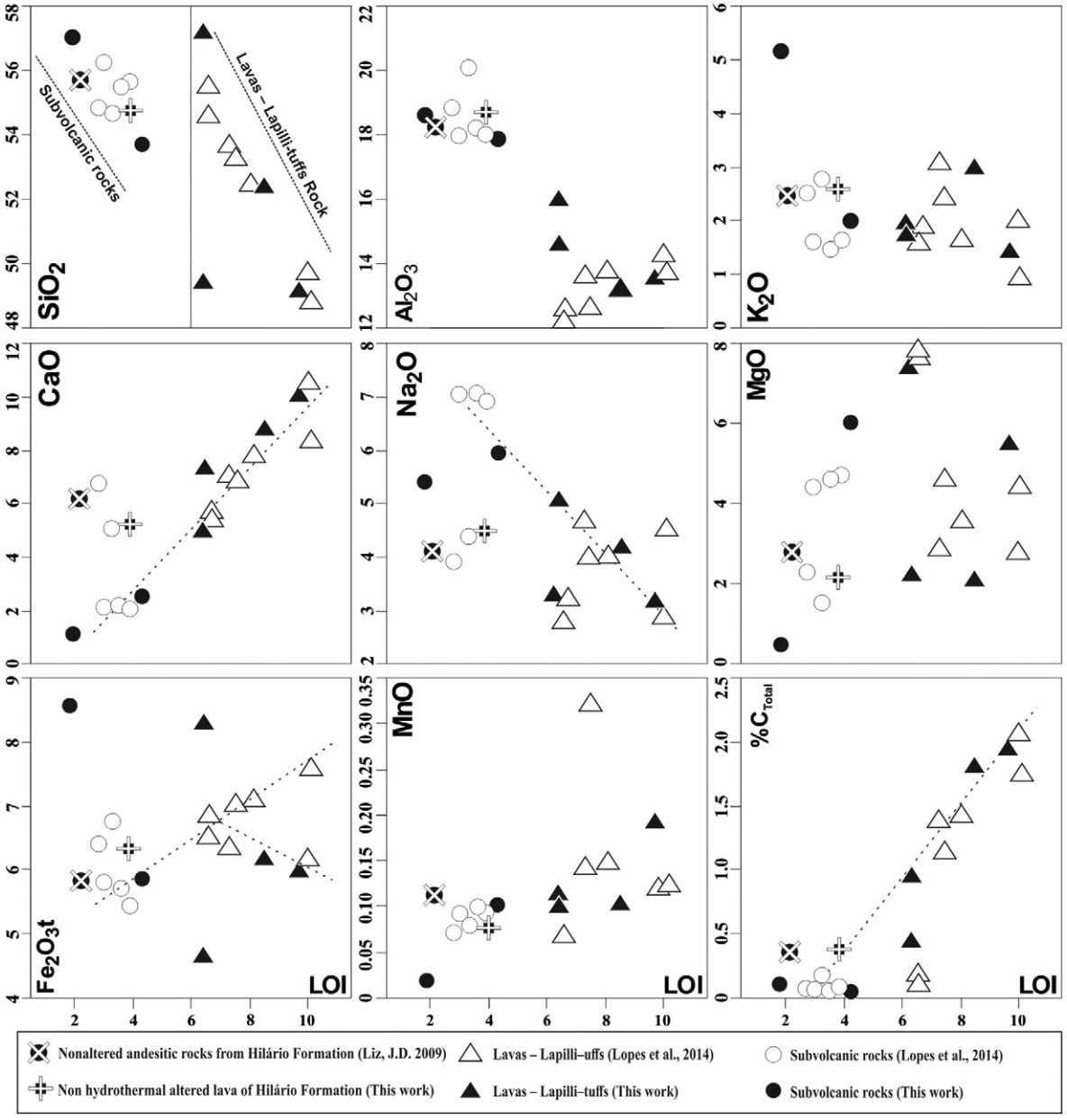

Fig. 8. Whole–rock variation diagrams: major and C_{total} vs. LOI (Table 1).

the presence of 10% to 20% of pressurized gas in the moment of Cal–3 formation. These textural and mineralogical changes show a chronological sequence of alteration where precipitations of S and S–rich C/S, corrensite and corrensite + calcite later formation. Consequently, corrensite precipitation is related to subvolcanic rocks chemical composition and water/rock chemistry or thermal changes. Since corrensite and C/S were recognized both as mixed layers, the precipitation from irregular S–rich C/S to corrensite was interpreted as a change of ordering related to a higher enthalpy conditions (C/S: Inoue et al., 1984; C: Hoffman and Hower, 1979; April, 1981; Horton, 1985; Bettison and Schiffman, 1988; Kameda et al., 2011; Vidal et al., 2012; Schleicher et al., 2013). These interpretations suggest i) temperature higher in SR than surrounding rocks, or ii) fluid circulation through fractures associated with calcite precipitation or a combination of (i) and (ii). Arguments in favor of scenario (i) are: a) occurrence of dominant corrensite in subvolcanic rocks replacing augite or amphibole shape filled of C/S + calcite indicates Mg and Fe source related to mafic minerals; b) the chilled margin of subvolcanic rock, its predominant 'corrensitic' alteration, and smaller proportion of S–rich irregular C/S in surrounding rocks suggests a thermal alteration associated with sub–volcanic emplacement. Nevertheless, these smectite and C/S + corrensite fill a large proportion (20 to 50%) of the lapilli–tuff rocks. Both REE (Chapter 5.2) and mineralogical arguments suggest that pervasive and fluid migration proceed from successive 'chloritization processes' associated with lapilli tuff alteration (i + ii).

The chloritization process in volcaniclastic rocks involves transformation of smectite to chlorite with Fe–Mg enrichment compare to Al–Na–Ca loss (Greenough and Papezik, 1985; Inoue and Utada, 1991). The chloritization was recognized in the microlithic matrix, replacing pyroxenes with corrensite and calcite in lavas or filling fractures and vesicles with smectite and different proportions of chlorite/smectite mixed layers. The vesicules and fractures show particles with radial distribution (Fig. 4–C) associated with initial smectite, late C/S irregular, or S–rich C/S irregular to corrensite and chlorite in the mineralized fault zone (Fig. 2). A similar chloritization (Inoue et al., 1984) was in recognized in active geothermal field and interpreted as a series of transformations with segregation of different amounts of C relative to S in irregular C/S to corrensite and chlorite.

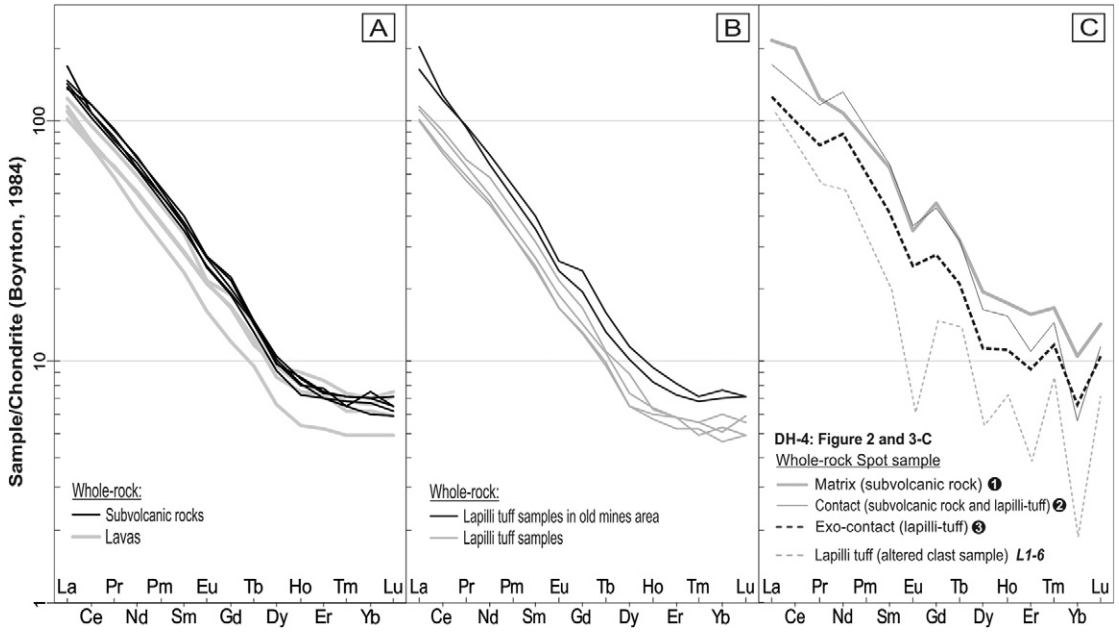

Fig. 9. REE normalized by chondrite values (Boynton, 1984). The samples and methods of this figure can be seen in Table 1.

The chloritization processes were previously studied in Volta Grande area, located several kilometers away from Seival Mines (Mexias et al., 1990). Al^{IV} values in Mg–chlorite suggested temperatures *c.* 300 °C related to propylitic to phyllic alteration in granitic and volcano–sedimentary contact zone. Al and Ca contents were added into the system due to the albitization process and Mg is from outside the system.

The corrensite occurrence and chloritization process (Briagatti and Poppi, 1984; Beaufort et al., 1997) were previously described in association with calcite + hematite. This association was also recognized in Hilário Formation (Mexias et al., 1990). This occurrence was related to an argillic alteration with a hydrocarbonic–rich fluid as suggested by the cogenetic precipitation of calcite. In the Lavras do Sul argillic

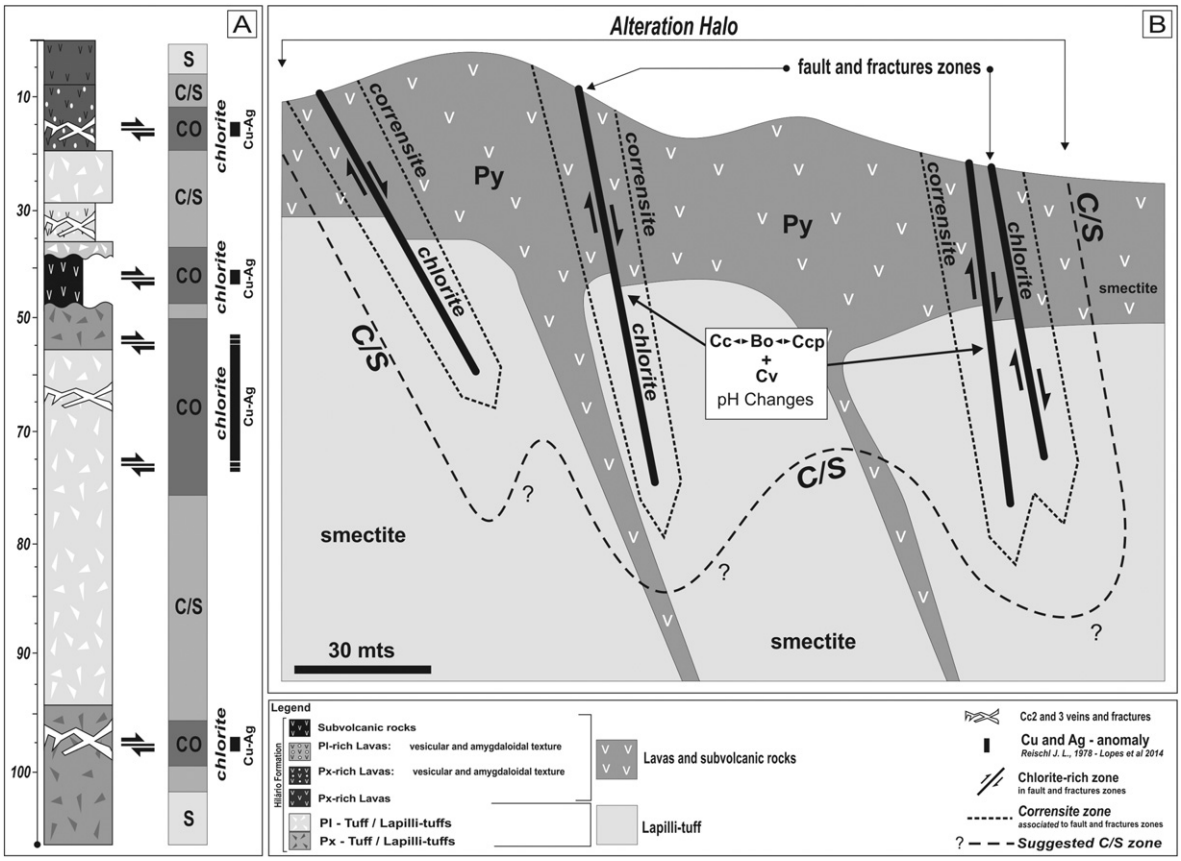

Fig. 10. Synthetic geological section and cross–section from Seival Mine area with fault and fractures alteration halos.

Table 1
Major and trace data from lapilli tuffs, lavas and subvolcanic rocks samples from Seival Mine volcanic rocks.

		Lopes et al., 2014											
	L[c]	SR					L				LT		
	SURFACE	L1-10	L1-4	DH4-24	DH4-25	DH4-26	DH24-28	DH24-29	L2-2	L2-1	L1-5	L1-2	L1-1
wt%													
SiO_2	55.7	54.7	54.79	56.21	55.63	55.45	55.58	54.67	53.6	53.25	52.41	49.74	48.8
Al_2O_3	18.3	20.05	18.83	18.01	18.04	18.22	12	12.51	13.59	12.61	13.77	14.27	13.7
K_2O	2.4	2.75	2.48	1.58	1.61	1.47	1.61	1.86	3.05	2.47	1.67	2.05	0.96
CaO	6.16	5.08	6.85	2.08	2.04	2.14	5.42	5.39	7	6.78	7.91	10.52	8.44
Na_2O	4.09	4.39	3.9	7.06	6.92	7.06	2.78	3.21	4.69	3.99	4.03	2.91	4.54
MgO	2.84	1.5	2.25	4.44	4.71	4.59	7.74	7.9	2.94	4.67	3.52	2.82	4.4
Fe_2O_{3T}	5.8	6.73	6.38	5.79	5.42	5.69	6.89	6.5	6.33	7.03	7.13	6.2	7.61
MnO	0.11	0.08	0.07	0.09	0.09	0.1	0.07	0.07	0.14	0.32	0.15	0.12	0.12
TiO_2	0.89	0.73	0.9	0.95	0.91	0.94	0.63	0.61	0.64	0.81	0.7	0.72	0.77
P_2O_5	0.34	0.31	0.37	0.47	0.44	0.46	0.25	0.25	0.25	0.32	0.27	0.27	0.28
LOI	2.2	3.3	2.8	3	3.9	3.6	6.6	6.6	7.3	7.5	8.1	10	10.1
$\%C_{Total}$	0.36	0.17	0.07	0.06	0.06	0.05	0.17	0.11	1.4	1.15	1.44	2.06	1.75
$\%S_{Total}$	0.28	<0.02	<0.02	<0.02	<0.02	<0.02	0.07	<0.02	<0.02	<0.02	<0.02	<0.02	<0.02
ppm													
Ba	1671.8	1832	1225	394	411	506	684	797	803	1082	844	880	272
Sr	1200.3	1215.4	1353.7	428.1	499	551.5	722.9	753.5	298	226.2	535.4	774.9	253.3
Rb	49.83	38.6	60.9	35.6	39.4	38.8	28.8	32.3	61.6	49.5	30.6	46.3	15.3
Cs		2.8	1.7	3.1	3	3.4	1.1	1	0.7	0.9	1.8	3.4	0.7
Ta		61	124	112	104	111	0.4	0.4	87	143	108	109	117
Nb	22	10.3	9.3	10.8	10.8	11.5	7.3	7.4	7.6	7.9	7.9	8.7	8.6
Th		11.3	10.2	12.3	11.5	12.6	5.2	5.5	6.1	8.4	5.9	7	5.8
U		3.9	3.7	4.5	4.3	4.7	2.1	2.2	2	2.9	2	2.6	3.2
Zr	296.6	187.4	168.9	190.1	189.6	194.5	124.7	125.8	143.4	149.8	137.4	155.6	139.3
V		10.1	15.1	13.9	13.4	13	99	100	27.3	19.5	26.2	30.2	32.7
Ga		19.4	26.9	5.6	4.1	2.9	16.7	17.2	13.8	8.2	4.7	5.2	2.8
Sc		N.A	N.A	N.A	N.A	N.A	15	14	N.A	N.A	N.A	N.A	N.A
Cu	N.A	71	62	231	141	77	28.4	33.9	62	76	62	35	38
Mo	N.A	0.6	0.5	0.9	0.4	0.7	0.5	0.6	0.7	0.8	0.3	0.4	0.2
Sn	N.A	2	2	2	2	2	1	1	1	1	1	2	2
W	N.A	1.9	1.1	0.9	0.7	1.1	1.1	<0.5	0.8	0.8	0.5	1	5.3
Zn	N.A	25.4	25	21.8	23	22.4	61	60	16.4	17.3	18.1	18.8	16.7
Pb	N.A	4.7	9.1	3.7	2.8	2.6	11.7	10.4	6.2	10.6	7.7	14.3	3.8
Ag	N.A	<0.1	<0.1	0.5	0.5	0.3	<0.1	<0.1	2.4	<0.1	<0.1	<0.1	<0.1
Ni	22.5	65.6	86.8	317	363.5	242.3	201.2	175.2	1355.7	55.2	27.1	22.9	52.1
Co	24.67	4.1	11.2	8.6	10.3	7.1	30.7	32	115.8	17	158.1	175.7	145.7
Se	N.A	<0.5	<0.5	<0.5	<0.5	<0.5	1	<0.5	<0.5	<0.5	<0.5	<0.5	<0.5
As	N.A	19.4	26.9	5.6	4.1	2.9	19.8	4.2	13.8	8.2	4.7	5.2	2.8
Sb	N.A	0.1	0.8	0.2	<0.1	<0.1	<0.1	0.1	0.2	0.2	<0.1	0.1	<0.1
Li	N.A	N.A	N.A	N.A	N.A	N.A	N.A	N.A	N.A	N.A	N.A	N.A	N.A
Tl	N.A	0.1	0.1	<0.1	<0.1	<0.1	0.2	0.2	<0.1	<0.1	<0.1	<0.1	<0.1
Hg	N.A	0.09	<0.01	0.28	0.2	0.18	0.33	0.11	0.1	<0.01	<0.01	<0.01	0.03
Au[b]	N.A	2.7	5.5	7.2	4.4	3.6	<0.5	1.5	1.9	4.1	1.8	0.8	1.5
La	52.14	44.3	42.5	46.2	42.2	54.9	30.7	31.5	31.5	38	31.4	34.6	35.4
Ce	102.73	87	82.3	97.1	93.7	105.7	59.5	61.2	63	77.2	64.9	68.7	72.8
Pr	10.62	10.16	9.75	11.11	11.07	11.86	6.87	7.14	7.07	9.2	7.6	7.84	8.37
Nd	43.21	40.1	37.5	42	42.6	45.1	26.8	27.8	25.3	35.3	29.7	29.6	34.6
Sm	8.9	7.18	6.76	7.25	7.39	7.56	4.82	4.73	4.57	6.59	5.43	5.24	6.07
Eu	2.03	1.79	1.84	1.79	1.96	1.99	1.23	1.22	1.18	1.6	1.56	1.38	1.59
Gd	6.52	4.86	4.98	4.98	5.2	5.18	3.43	3.39	3.14	4.87	3.95	3.69	4.29
Tb	N.A	0.63	0.69	0.7	0.7	0.68	0.47	0.45	0.45	0.68	0.53	0.51	0.52
Dy	3.88	2.92	3.15	3.27	3.27	3.27	2.11	2.1	2.14	3.1	2.77	2.38	2.86
Ho	0.71	0.52	0.62	0.56	0.58	0.52	0.41	0.43	0.39	0.65	0.51	0.46	0.45
Er	1.92	1.47	1.58	1.54	1.48	1.59	1.11	1.22	1.11	1.74	1.43	1.22	1.23
Tm	0.33	0.21	0.23	0.24	0.22	0.23	0.17	0.16	0.16	0.24	0.19	0.18	0.18
Yb	1.5	1.57	1.47	1.45	1.41	1.3	0.97	1.11	1.03	1.46	1.2	1.06	1.26
Lu	0.25	0.21	0.21	0.2	0.2	0.19	0.16	0.16	0.16	0.24	0.18	0.19	0.18
La/Yb	34.74	28.22	28.91	31.86	29.93	42.23	31.65	28.38	30.58	26.03	26.17	32.64	28.1
Eu/Eu[a]	0.8	0.92	0.97	0.91	0.97	0.97	0.93	0.93	0.95	0.86	1.03	0.96	0.95
ΣREE	234.5	202.9	193.5	218.39	211.98	240.07	138.75	142.61	141.2	180.87	151.35	157.05	169.8

[a] Lava of Hilário Formation (background).
[b] Values for Au = ppb.
[c] Nonaltered andesitic rocks from Hilário Formation (Liz. J.D. 2008).

alteration, the cogenetic precipitation of corrensite and calcite were related to a temperature range of 130 to 280 °C (Meunier et al., 1988; Mexias et al., 1990). In the Seival Mine area, the occurrence of corrensite and calcite with H_2O and CO_2 fluid inclusion supports similar interpretation. However, in the altered volcanic rocks of Seival Mine area, corrensite + calcite + hematite occurs associated with faults and fractures in alteration halos. Following Meunier et al. (1988) and Mexias et al. (1990), the high Fe^{3+} content in corrensite and its coexistence with hematite indicate redox changes (Eh–pH) most probably related to an increasing oxygen fugacity.

This work														
L[a]	L					LT-tuff	LT-alt.clast	LT-clast	SR	SR-matrix	SR-W.R.	SR-matrix	SR-contat	SR-tuff
SURFACE	DH4-20	DH24-22	DH3-13	L1-6	L1-7	L1-8			L1-3	DH3-15	DH4-26			
wt%														
54.74	49.1	N.A	49.41	52.4	57.22	N.A	N.A	N.A	57.07	N.A	53.65	N.A	N.A	N.A
18.73	13.56	N.A	14.58	13.16	16	N.A	N.A	N.A	18.54	N.A	17.87	N.A	N.A	N.A
2.64	1.46	N.A	1.68	2.96	1.91	N.A	N.A	N.A	5.16	N.A	1.96	N.A	N.A	N.A
5.26	9.97	N.A	7.31	8.76	4.97	N.A	N.A	N.A	1.1	N.A	2.51	N.A	N.A	N.A
4.52	3.21	N.A	3.24	4.15	5.04	N.A	N.A	N.A	5.42	N.A	5.95	N.A	N.A	N.A
2.13	5.49	N.A	7.5	2.04	2.18	N.A	N.A	N.A	0.51	N.A	5.99	N.A	N.A	N.A
6.31	6.01	N.A	8.28	6.19	4.63	N.A	N.A	N.A	8.57	N.A	5.84	N.A	N.A	N.A
0.08	0.19	N.A	0.1	0.1	0.11	N.A	N.A	N.A	0.02	N.A	0.1	N.A	N.A	N.A
0.9	0.75	N.A	0.79	0.98	0.93	N.A	N.A	N.A	0.81	N.A	0.97	N.A	N.A	N.A
0.35	0.25	N.A	0.26	0.46	0.31	N.A	N.A	N.A	0.32	N.A	0.46	N.A	N.A	N.A
3.9	9.7	N.A	6.4	8.5	6.4	N.A	N.A	N.A	1.9	N.A	4.3	N.A	N.A	N.A
0.4	1.93	N.A	0.43	1.79	0.97	N.A	N.A	N.A	0.1	N.A	0.04	N.A	N.A	N.A
<0.02	<0.02	N.A	<0.02	<0.02	<0.02	N.A	N.A	N.A	<0.02	N.A	0.03	N.A	N.A	N.A
ppm														
1580	410	103.85	794	783	248	791.01	511.56	567.47	3270	686.26	777	428.44	556.46	2471.27
1241.3	508.5	108.14	753.1	289.9	187.6	194.99	199.7	226.84	896.4	407.99	632.6	515.24	570.5	4601.93
56	26.7	19	34.7	53.4	63.1	55.18	36.91	37.2	131.5	58.98	50.1	33.15	40.84	91.74
6.2	2.1	N.A	1.5	1.5	5.6	N.A	N.A	N.A	5	N.A	4	6.82	N.A	30.49
2.9	0.5	1.07	0.5	0.6	0.5	n.d.	n.d.	n.d.	0.3	n.d.	0.8	12.54	16.87	234.56
9.2	7	16.85	7.4	10.7	9	35.72	31.55	36.2	7.5	41.93	11	43.4	48.93	176.38
9.4	4.8	N.A	5.6	10.4	7.8	N.A	N.A	N.A	6.5	N.A	12.2	N.A	N.A	N.A
3.3	1.9	6.11	2.3	4.1	2.9	11.79	9.39	13.31	2.2	18.37	4.8	15.79	17.09	60.65
167.3	129.6	169.1	143.9	195.3	163	213.3	203.8	219.51	145.4	278.03	194.7	295.79	312.62	1509.39
127	128	150.06	134	115	159	n.d.	n.d.	n.d.	162	n.d.	121	187.6	n.d.	1372.1
22.4	15.9	26.27	18.6	12.6	21.4	88.16	64.09	70.27	21.3	86.4	22.7	64.14	73.66	412.29
N.A	17	N.A	17	16	23	N.A	N.A	N.A	13	N.A	11	N.A	N.A	N.A
86.8	48.4	287.97	30.9	62.3	75.2	n.d.	4970.11	n.d.	2.1	190.88	522.3	4881.11	3929.36	n.d.
0.3	<0.1	23.52	0.5	0.4	<0.1	71.97	54.44	81.05	0.3	109.19	0.4	77.69	83.2	381.78
2	1	N.A	1	3	2	N.A	N.A	N.A	1	N.A	1	N.A	N.A	N.A
1.6	0.8	N.A	0.6	2	1.2	N.A	N.A	N.A	1.4	N.A	1.4	N.A	N.A	55.33
66	137	831.16	76	42	38	n.d.	n.d.	n.d.	22	n.d.	180	n.d.	n.d.	900.89
16.7	4.7	9.68	28.7	14.3	1.9	14.67	17.66	16.44	14.1	15.25	2.6	21.81	24.23	74.27
0.1	<0.1		<0.1	0.7	<0.1	N.A	N.A	N.A	<0.1	N.A	0.5	N.A	N.A	N.A
9.6	108.2	100.87	92.5	127.4	106.8	309.51	1684.66	5003.68	42.1	212.25	10.6	101.21	524.94	3745.43
15.7	28.8	61.01	32	21.7	10.4	35.59	91.27	76.22	13	21.59	15	33.56	51.93	330.29
<0.5	<0.5	N.A	<0.5	<0.5	<0.5	N.A	N.A	N.A	<0.5	N.A	<0.5	N.A	N.A	N.A
21.8	1.2	9.1	5.4	22	1.1	29.15	12.68	18.86	14.5	N.A	5.4	N.A	7.39	135.89
1.6	<0.1	N.A	0.4	1.8	<0.1	N.A	N.A	N.A	0.6	N.A	0.2	N.A	N.A	N.A
N.A	N.A	36.06	N.A	N.A	N.A	30.6	38.5	38.7	N.A	45.9	N.A	44.1	38.02	358.14
<0.1	<0.1	N.A	<0.1	<0.1	<0.1	N.A	N.A	N.A	<0.1	N.A	<0.1	N.A	N.A	N.A
0.06	0.02	N.A	0.01	0.18	3.56	N.A	N.A	N.A	<0.01	N.A	0.13	N.A	N.A	N.A
4.2	1.9	N.A	<0.5	0.6	<0.5	N.A	N.A	N.A	<0.5	N.A	3.2	N.A	N.A	N.A
46.5	33.6	30.92	35.7	50.2	62.6	25.67	33.28	31.41	51.9	78.61	45.4	66.54	52.52	39
88.7	63.3	65.08	65.4	97.7	102.2	59.46	61.66	62.79	86.7	174.12	94.2	160.82	114.44	80.86
10.27	7.88	7.25	7.79	11.53	11.38	7.19	6.66	7.19	10.47	16.01	11.2	15.02	14.14	9.69
38.7	29.9	36.74	30.5	43.2	39.2	33.26	30.92	33.75	37.9	70.34	41.8	64.31	78.85	52.64
7.1	5.49	7.04	5.53	7.78	6.91	3.91	3.84	4.47	7.33	13.42	7.77	12.46	12.74	8.09
1.96	1.54	1.45	1.56	1.92	1.74	0.2	0.45	0.53	1.99	3.77	1.99	2.55	2.7	1.83
5.3	4.41	7.27	4.3	6.14	5	3.63	3.8	4.3	5.64	12.69	5.76	11.66	11.22	7.22
0.66	0.59	0.77	0.55	0.75	0.63	0.96	0.66	0.87	0.68	1.49	0.7	1.51	1.51	1
3.55	2.77	3.99	3.1	3.72	3.3	1.63	1.75	2.45	3.19	6.02	3.4	6.27	5.31	3.66
0.6	0.54	0.64	0.57	0.68	0.59	0.74	0.52	0.75	0.57	1.1	0.61	1.25	1.1	0.8
1.61	1.52	2.13	1.57	1.69	1.53	0.54	0.81	1.27	1.62	3.1	1.54	3.27	2.31	1.94
0.22	0.2	0.23	0.22	0.23	0.22	0.45	0.28	0.41	0.21	0.46	0.23	0.54	0.47	0.38
1.53	1.3	1.66	1.39	1.58	1.48	b.d.l.	0.39	0.82	1.26	2.19	1.48	2.18	1.18	1.39
0.2	0.19	0.21	0.23	0.23	0.23	0.36	0.23	0.36	0.19	0.42	0.23	0.46	0.37	0.34
30.39	25.85	18.61	25.68	31.77	42.3		84.9	38.47	41.19	35.87	30.68	30.5	44.32	28.15
0.97	0.95	0.62	0.97	0.84	0.9	0.17	0.36	0.37	0.95	0.88	0.9	0.65	0.69	0.73
206.9	153.2	165.4	158.4	227.3	237	138	145.23	151.37	209.65	383.7	206.3	348.85	298.87	208.83

6.4. Alteration halos and Cu–sulfide minerals in fractures

The N–NE ruptile structures, as previously discussed, are considered as a system of strike–slip faults (Fig. 1–B). The strong hydrothermal events that affected the Seival Mines volcanic rocks and caused the occurrence of hydraulic breccia and mineralization is associated with these lineaments. According to Reischl (1978) and Lopes et al. (2014) and this work, the mineralizations are associated with circulation of hydrothermal and supergene fluids in these structures. The alteration halos are marked by the occurrence of irregular mixed layers (C/S)

and later corrensite, frequently associated with structures and fluid circulation. Relations between the lithology and hydrothermal alteration distribution in these fault zones led us to suggest a vertical recharge process. The multiple generation of calcite veins (Cal–2 and 3) record the hydrothermal changes associated with the emplacement and cooling of subvolcanic rocks or represent later calcite precipitations in lapilli–tuff – subvolcanic rocks contact. Additionally, the corrensite and Cal–3 association suggests that Cal–3 calcite formed under temperatures between 130 and 280 °C, which represents cooler hydrothermal stages. Some fluid inclusions in Cal–3 contain 10 to 20% of liquid CO_2 (apparent proportion). The lack of mineralogical evidences of boiling suggests the homogeneity of $H_2O + CO_2$ fluid. The $H_2O - CO_2$ liquid separation can occur from 10 to 100 MPa for temperatures higher than 210 °C. Considering this range of pressures, the fluid inclusions in Cal–3 veins exposed from the surface down to approximately 500 m deep were, in fact, formed at depths >500 m. The petrography, mineral chemistry and relative chronology of sulfides and its distribution in alteration halos led us to suggest the following evolutional model. The hydrothermal Cu–Fe sulfide precipitation is observed in at least two stages: i) related to the post–magmatic fluids of subvolcanic rocks and lavas and, therefore, associated with higher temperature conditions, low Cu/S activity ratio, and, presumably more reducing conditions; ii) haloes with hematite and chalcocite–covellite in lavas–lapilli–tuff.

The sulfide textures observed in alteration halos reveal complex intergrowths and partial replacements by covellite (supergenic stage). The change of Cu/S activity ratio might be related to pH changes (Reed and Palandri, 2006). In such case, the presence of larger amount of disseminated chalcocite in alteration halos from Seival Mines would be related to fluids with low pH (*c.* 3). The clay mineral associated with sulfide would then represent the reaction of intermediate rocks with acid fluids (Meyer and Hemley, 1968). This pH increase is associated to reaction of hydrothermal fluids with volcanic wall rocks altering feldspars and forming carbonates. The CO_2 gas may be responsible for the reduction of H^+ activity and consequently cooling of fluids.

The presence of covellite (covelitte + chalcocite – covellite + chalcopyrite – Fig. 7) in the core of Seival Mines alteration halos indicates a more acidic and oxidant condition during the supergenic stages. Changes in oxidation conditions of a hydrothermal system are accompanied by (i) changes in the stability of sulfide minerals, and (ii) chalcocite common association with covellite in low–pH supergene environments. The supergenic enrichment zones are commonly developed in porphyry Cu deposits (Anderson, 1982). In the volcanic and pyroclastic rocks of porphyry Cu deposit (SE–Iran), immature supergene zones were described, and are distinguished mainly by the increase in contents of chalcocite and covellite (Afzal et al., 2016).

During the later stages of alteration halos development (L1–1, 6 and 7), barite veins were formed, representing the sulphated phase of the system, with lower temperatures and increasing oxidation as discussed by Arribas (1995).

7. Conclusions

The volcanic and sub-volcanic rocks associated with the hydrothermal system in the Seival Mine area represent the early magmatic stages of the Lavras do Sul magmatic system. The volcanic rocks have not been affected by the thermal metamorphic halo (Mexias et al., 1991a, 1991b) near plutons associated with dikes and hydrothermal alteration along the strike–slip fractures of the Camaquã basin.

Post–volcanic alteration dominantly produced albitization and early smectite crystallization that is petrographically related to late magmatic fluids. This alteration covers a temperature domain from *c.* 300 °C (albitization–epidote + titanite) to *c.* 80 °C (chamosite/saponite). The porous lapilli tuff to compact lavas exhibit smectite or chlorite/smectite precipitation. The ubiquitous occurrence of chlorite/smectite mixed layers suggests a hydrothermal alteration related to lava flow emplacement or fluid drainage through porous material. The precipitation of corrensite and calcite assemblages in fractures that crosscut or overprint chlorite–smectite altered rocks seem to form halo associated with dike cooling and fluid circulation along the lava flow–dike discontinuity. The trioctahedral chlorite dominates in fractures associated with sulfide and calcite.

The normative C.I.P.W. calculation for post–magmatic alteration mineral assemblages produced albite and saponite (Na) beside illite (K). Calculated hydrothermal to supergene phases were calcite, chamosite/saponite mixed layers (Ca, Fe and Mg) and Al–rich chlorite. A modal composition of altered rocks (Chapter 5.1) indicates that albitized volcanic rocks contain up to two thirds of alteration (clays and calcite). Among the different modal phases, a number record the occurrence of illite characterized by XRD or K–feldspar. Smectite, chlorite/smectite and corrensite with illite and calculated K–feldspar suggest formation in a system of argillic alteration related to a decrease in temperature of cooling lavas, fluid circulation and emplacement of sub-volcanic rocks.

These clay minerals pervasively overprint the original lavas and contain minor Cu–rich sulfide. The chlorite/smectite and Cu–rich sulfides seem to represent a hydrous–Cu–rich supergene or peripheral enrichment when compared to the chlorite and sulfide rich fractures. Further work will attempt to characterize the chemistry of the meteoric or magmatic source fluid with the relative chronology. The chemical transitional environment, marked by pH variations and covelitte–chalcocite–bornite–chalcopyrite occurrence, allows the suggestion of a dynamic dispersion of post–magmatic to late circulation of metals in hydrothermal fluids in fractures.

Acknowledgments

This study was partly funded by CAPES–COFECUB (project n°619/08) and a personal grant to C. Renac from UNICE/GEOAZUR. The authors thank VOTORANTIN metal company for borehole samples. We thank Michel Manetti (*in memorian*) for his help during the sampling strategy steps of this work and friendly moments.

References

Afzal, P., Tehrani, M.E., Ghaderi, M., Hosseini, M.R., 2016. Delineation of supergene enrichment, hypogene and oxidation zones utilizing staged factor analysis and fractal modeling in Takht–e–Gonbad porphyry deposit, SE Iran. J. Geochem. Explor. 161, 119–127.

Anderson, J.A., 1982. Characteristics of leached capping and techniques of appraisal. In: Titley, S.R. (Ed.), Advances in Geology of Porphyry Copper Deposits, Southwestern North America. University Arizona Press, Tucson, pp. 275–295.

April, R.H., 1981. Trioctahedrat smectite and interstratified chlorite/smectite in Jurassic strata of the Connecticut Valley. Clay Clay Miner. 29, 31–39.

Arribas Jr., A., 1995. Characteristics of high–sulfidation epithermal deposits and their relation to magmatic fluid. Mineral. Assoc. Can. Short Course 23, 419–454.

Barbosa, A.F., 1958. Alguns aspectos da mineralização de cobre e da pesquisa das jazidas do Seival, Estado do Rio Grande do Sul. Tese apresentada a Comissão Julgadora do Concurso à Catedra de Jazidas Minerais. da Escola Politécnica da Universidade de São Paulo, Legislação de Minas.

Barth, T.F.W., 1955. Presentation of rock analyses. J. Geol. 63, 348–363.

Beaufort, D., Meunier, A., 1994. Saponite, corrensite and chlorite/saponite mixed–layered minerals and saponite in the Sancerre–Couy deep drill hole (France). Clay Miner. 29, 47–61.

Beaufort, D., Baronnet, A., Lanson, B., Meunier, A., 1997. Corrensite: a single phase or a mixed layered phyllosilicate of the saponite–chlorite conversion series? The case study of the Sancerre–Couy deep drill–hole (France). Am. Mineral. 82, 109–124.

Bettison, L.A., Schiffman, R., 1988. Compositional and structural variations of phyllosilicates from the Point Sal ophiolite, California. Am. Mineral. 73, 62–76.

Bettison-Varga, L., Mackinnon, I.D.R., 1997. The role of randomly mixed–layered chlorite/smectite in the transformation of smectite to chlorite. Clay Clay Miner. 45, 506–516.

Bitencourt, M.F., Nardi, L.V.S., 1993. Late to post-collisional Brasiliano granitic magmatism in southernmost Brazil. Anais da Academia Brasileira de Ciência 65 (1), 3–16.

Boles, J.R., 1982. Active albitization of plagioclase, gulf–coast tertiary. Am. J. Sci. 282, 165–180.

Bongiolo, E.M., Bongiolo, D.E., Sardini, P., Mexias, A.S., Siitari-Kauppi, M., Gomes, M.E.B., Formoso, M.L.L., 2007. Quantification of porosity evolution from unaltered to propylitic–altered granites: the 14C–PMMA method applied on the hydrothermal system of Lavras do Sul, Brazil. An. Acad. Bras. Cienc. 79, 503–517.

Bongiolo, E.M., Patrier-Mas, P., Mexias, A.S., Beaufort, D., Formoso, M.L.L., 2008. Spatial and temporal evolution of hydrothermal alteration at Lavras do Sul, Brazil: evidence from dioctahedral clay minerals. Clay Clay Miner. 56, 222–243.

Bongiolo, E.M., Renac, C., Mexias, A.S., Gomes, M.E.B., Ronchid, L.H., Patrier-Mase, P., 2011. Evidence of Ediacaran glaciation in southernmost Brazil through magmatic to meteoric fluid circulation in the porphyry–epithermal Au–Cu deposits of Lavras do Sul. Precambrian Res. 189, 404–419.

Borba, A.W., Mizusaki, A.M.P., Santos, J.O.S., McNaughton, N.J., Onoe, A.T., Hartmann, L.A., 2008. U–Pb zircon and ^{40}Ar–^{39}Ar K–feldspar dating of syn–sedimentary volcanism of the Neoproterozoic Maricá formation: constraining the age of foreland basin inception and inversion in the Camaquã Basin of southern Brazil. Basin Res. 20, 359–375.

Boynton, W.V., 1984. Geochemistry of the rare earth elements: meteorite studies. In: Henderson, P. (Ed.), Rare Earth Element Geochemistry. Elsevier, Amsterdam, pp. 63–114.

Briagatti, M.F., Poppi, L., 1984. Crystal chemistry of corrensite: a review. Clay Clay Miner. 32 (5), 391–399.

Brito Neves, B.B., Cordani, U.G., 1991. Tectonic evolution of South America during late Proterozoic. Precambrian Res. 53, 23–40.

Carvalho, P.F., 1932. Reconhecimento Geológico do Estado do Rio Grande do Sul. Boletim do Serviço Geológico e Mineralógico do Brasil 66, 1–72.

Chemale Jr., F., 2000. Evolução Geológica do Escudo Sul–rio–grandense. In: Holz, M., De Ros, L.F. (Eds.), Geologia do Rio Grande do Sul. Ed. da Universidade/UFRGS, Porto Alegre, pp. 13–52.

Chemale Jr., F., Hartmann, L.A., da Silva, L.C., 1995. Stratigraphy and tectonism of Brasiliano Cycle in southern Brazil. Commun. Geol. Surv. Namibia 10, 151–166.

Cross, W., Iddings, J.P., Pirson, L.V., Washington, H.S., 1902. A quantitative chemicomineralogical classification and nomenclature of igneous rocks. J. Geol. 10, 555–690.

De La Roche, H., Leterrier, J.T., Grandclaude, P., Marchal, M., 1980. A classification of volcanic and plutonic rocks using R1–R2 diagram and major–element analyses–its relationships with current nomenclature. Chem. Geol. 29, 183–210.

Farmer, V.C., Krishnamurti, G.S.R., Huang, R.M., 1991. Synthetic allophane and layer–silicate formation in SiO_2–$A1_2O_3$–FeO–Fe_2O_3–MgO–H_2O systems at 23~ and 89~ in a calcareous environment. Clay Clay Miner. 39, 561–570.

Farmer, V.C., McHardy, W.J., Elsass, E., Robert, M., 1994. hk–ordering in aluminous nontronite and saponite synthesized near 90°C effects of synthesis conditions on nontronite composition and ordering. Clay Clay Miner. 42, 180–186.

Fragoso-Cesar, A.R.S., Faccini, U.F., Paim, P.S.G., Lavina, E.L., Altamirano, J.A.F., 1985. Revisão na estratigrafia das molassas do Ciclo Brasiliano no Rio Grande do Sul. Anais do Simpósio Sul–Brasileiro de Geologia, Florianópolis, pp. 477–491.

Gastal, M.C.P., 1999. The alkaline and shoshonitic intrusives in the region of the Taquarembó Plateau, southern Brazil: Are they genetically related? Braz. J. Geol. 29, 85–98.

Gastal, M.C.P., Ferreira, F.J.F., da Cunha, J.U., Esmeris, C., Koester, E., Raposo, M.I.B., Rossetti, M.M.M., 2015. Alojamento do granito Lavras e a mineralização aurífera durante evolução de centro vulcano–plutônico pós–colisional, oeste do Escudo Sul–riograndense: Dados geofísicos e estruturais. Braz. J. Geol. 45, 217–241.

Gastal, M.C.P., Lafon, J.M., 1998. Gênese e evolução dos granitóides metaluminosos de afinidade alcalina da porção oeste do escudo Sul–riograndense: geoquímica e isótopos de Rb–Sr e Pb–Pb. Braz. J. Geol. 28, 9–28.

Gastal, M.C.P., Lafon, J.M., Hartmann, L.A., Koester, E., 2005. Sm–Nd isotopic compositions as a proxy for magmatic process during the Neoproterozoic of the southern Brazilian shield. J. S. Am. Earth Sci. 18, 255–276.

Gavronski, E.F., 1963. Relatório de Sondagem de 1962–63 no setor Barita da Mina do Seival (Divisão de Fomento da Produção Mineral do DNPM/Companhia Brasileira do Cobre. – Inédito – Porto Alegre).

Goni, J.C., Goso, H., Issler, R.S., 1962. Estratigrafia e Geologia econômica do Pré–cambriano e Eo–paleozóico uruguaio e sul–riograndense. Boletim da Escola de Geologia UFRGS 3, 1–105.

Greenough, J.D., Papezik, V.S., 1985. Petrology and geochemistry of Cambrian volcanic rocks from the Avalon Peninsula, Newfoundland. Can. J. Earth Sci. 22, 1594–1601.

Hallinan, S.E., Mantovani, M.S.M., Shukowski, W., Braggion Jr., I., 1993. Estrutura do Escudo Sul–brasileiro: uma revisão através de dados gravimétricos e magnetométricos. Braz. J. Geol. 23, 201–214.

Hartmann, L.A., Philipp, R.P., Santos, J.O.S., McNaughton, N.J., 2011. Time frame of 753–680 Ma juvenile accretion during the São Gabriel orogeny, southern Brazillian Shield. Gondwana Res. 19 (1), 84–99.

Hoffman, J., Hower, J., 1979. Clay mineral assemblages as low–grade metamorphic geothermometers, application to the thrust faulted disturbed belt of Montana, USA. Soc. Econ. Paleontol. Mineral. Spec. Pap. 26, 55–79.

Horton, D.G., 1985. Mixed layer illite/smectite as a paleotemperature indicator in the Amethyst vein system. Creede district, Colorado, USA. Contrib. Mineral. Petrol. 91, 171–179.

Hövelmann, J., Putnis, A., Geisler, T., Schmidt, B.C., Golla-Schindler, U., 2010. The replacement of plagioclase feldspars by albite: observations from hydrothermal experiments. Contrib. Mineral. Petrol. 159, 43–59.

Inoue, A., 1987. Conversion of smectite to chlorite by hydrothermal and diagenetic alterations, Hokuroku Kuroko mineralization area, northeast Japan. In: Schultz, L.G., van Olphen, H., Mumpton, F.A. (Eds.), Proceedings of the International Clay Conference. The Clay Minerals Society, Denver, pp. 158–164.

Inoue, A., Utada, M., 1991. Smectite to chlorite transformation in thermally metamorphosed volcanoclastic rocks in the Kamikita area, northern Honshu, Japan. Am. Mineral. 76, 628–640.

Inoue, A., Utada, M., Nagata, H., Watanabe, T., 1984. Conversion of trioctahedral smectite to interstratified chlorite/smectite in Pliocene acidic pyroclastic sediments of the Ohyu district, Akita Prefecture, Japan. Clay Sci. 6, 103–106.

Janikian, L., de Almeida, R.P., da Trindade, R.I.F., Fragoso-Cesar, A.R.S., D'Agrella-Filho, M.S., Dantas, E.L., Tohver, E., 2008. The continental record of Ediacaran volcano–sedimentary successions in southern Brazil and their global implications. Terra Nova 20, 259–266.

Janikian, L., Almeida, R.P., Fragoso-Cesar, A.R.S., Martins, V.T.S., Dantas, E.L., Tohver, E., McReath, I., D'Agrella-Filho, M.S., 2012. Ages (U–Pb SHRIMP and LA–ICP–MS) and stratigraphic evolution of the Neoproterozoic volcano–sedimentary successions from the extensional Camaquã Basin, southern Brazil. Gondwana Res. 21, 466–482.

Johannsen, A., 1931. A Descriptive Petrography of the Igneous Rocks. Vol. 1. University of Chicago Press, Chicago.

Kackstaetter, U.R., 2014. SEDMIN–Microsoft Excel™ spreadsheet for calculating fine–grained sedimentary rock mineralogy from bulk geochemical analysis. Cent. Eur. J. Geosci. 6 (2), 170–181.

Kameda, J., Ujiie, K., Yamaguchi, A., Kimura, G., 2011. Smectite to chlorite conversion by frictional heating along a subduction-zone thrust. Earth Planet. Sci. Lett. 305, 161–170.

Le Maitre, R.W., Streckeisen, A., Zanettin, B., Le Bas, M.J., Bonin, B., Bateman, P. (Eds.), 2005. Igneous Rocks: A Classification and Glossary of Terms: Recommendations of the International Union of Geological Sciences Subcommission on the Systematics of Igneous Rocks, second ed. Cambridge University Press, New York.

Lee, M.R., Parsons, I., 1997. Dislocation formation and albitization in alkali feldspars from the Shap granite. Am. Mineral. 82, 557–570.

Leinz, V., 1946. Teores em ouro e prata no minério de Cobre de Camaquã e Seival, Município de Caçapava do Sul, Rio Grande do Sul. Min. e Metal. 9, 1–60.

Leinz, V., Barbosa, A.F., Teixeira, E.A., 1947. Mapa Geológico Caçapava – Lavras, Rio Grande do Sul. Divisão de Produção Mineral, Bol. 9, 1–90.

Lima, E.F., Nardi, L.V.S., 1998a. The Lavras do Sul shoshonitic association: implications for origin and evolution of eoproterozoic shoshonitic magmatism in southermost Brazil. J. S. Am. Earth Sci. 11, 67–77.

Lima, E.F., 1995. Petrologia das Rochas Vulcânicas e Hipoabissais da Associação Shoshonítica de Lavras do Sul – ASLS, RS. Doctoral Thesis. IGc–UFRGS, Porto Alegre (338 pp).

Lima, E.F., Nardi, L.V.S., 1998b. Química mineral das rochas vulcânicas e lamprófiros espessartíticos da Associação Shoshonítica de Lavras do Sul–RS. Braz. J. Geol. 28, 113–124.

Liz, J.D., Lima, E.F., Nardi, L.V.S., 2009. Avaliação de fontes magmáticas de series shoshoníticas pós–colisionais com base na normalização pela Associação Shoshonítica de Lavras do Sul – aplicação de Sliding Normalization. Braz. J. Geol. 39, 55–66.

Lopes, W.R., Fontana, E., Mexias, A.S., Gomes, M.E.B., Nardi, L.V.S., Renac, C., 2014. Caracterização petrográfica e geoquímica da sequência magmática da Mina do Seival, Formação Hilário (Bacia do Camaquã – Neoproterozóico), Rio Grande do Sul, Brasil. Revista Pesquisas em Geociências 41, 51–64.

Machado, R., Fragoso-Cesar, A.R.S., 1987. Deformações brasilianas do cinturão Dom Feliciano no Uruguai. Anais do Simpósio Sul–Brasileiro de Geologia, Curitiba, pp. 911–919.

Melcher, C., Mau, H., 1960. Novas observações geológicas na região de Caçapava do Sul, Rio Grande do Sul. An. Acad. Bras. Cienc. 32, 43–50.

Meunier, A., 2005. Clays. first ed. Springer, Berlin.

Meunier, A., Clement, J.Y., Bouchet, A., Beaufort, D., 1988. Chlorite–calcite and corrensite–dolomite crystallization during two superimposed events of hydrothermal alteration in the "Les Cretes" granite, Vosges, France. Can. Mineral. 26, 413–442.

Mexias, A.S., Formoso, M.L., Gomes, M.E.B., Meunier, A., Beaufort, D., Mattos, I., 1991b. O Sistema Hidroterma; Fóssil de Volta Grande – Lavras do Sul/RS. Parte II – Geoquímica das Cloritas. Geochim. Bras. 4, 159–174.

Mexias, A.S., Formoso, M.L., Meunier, A., Beaufort, D., 1991a. O Sistema Hidrotermal Fóssil de Volta Grande – Lavras do Sul/RS. Parte I – Petrografia do Hidrotermalismo. Geochim. Bras. 4, 139–157.

Mexias, A.S., Formoso, M.L.L., Meunier, A., Beaufort, D., 1990. Composition and crystallization of corrensite in volcanic and pyroclastic rocks of Hilário Formation (RS) Brazil. Sci. Géol. 88, 135–143.

Mexias, A.S., Berger, G., Gomes, M.E.B., Formoso, M.L.L., Dani, N., Frantz, J.C., Bongiolo, E.M., 2005. Geochemical Modelling of gold precipitation conditions in Bloco do Butiá Mine, Lavras do Sul/Brazil. An. Acad. Bras. Cienc. 77, 1–12.

Mexias, A.S., Bongiolo, E.M., Gomes, M.E.B., Formoso, M.L.L., Frantz, J.C., 2007. Alterações hidrotermais e mineralizações nas rochas da Associação Plutono–vulcano–Sedimentar da região de Lavras do Sul–RS. In: Ianuzzi, R., Frantz, J.C. (Eds.), 50 Anos de Geologia: Instituto de Geologia, Contribuições. ed. Comunicação e Identidade, Porto Alegre, pp. 143–159.

Meyer, C., Hemley, J., 1968. Wall rock alteration. In: Barnes, H.L. (Ed.), Geochemistry of Hydrothermal Ore Deposits, first ed. John Wiley & Sons, pp. 166–235.

Müller, I.F., Nardi, L.V.S., Lima, E.F., Mexias, A.S., 2012. Os diques latíticos portadores de ouro e sulfetos da Associação Shoshonítica de Lavras do Sul – RS: Petrogênese e Geoquímica. Revista Pesquisas em Geociências 39, 173–191.

Nardi, V.S.N., Lima, E.F., 1985. A Associação Shoshonítica de Lavras do Sul, RS. Braz. J. Geol. 15, 139–146.

Nardi, L.V.S., Lima, E.F., 1988. Hidrotermalismo no complexo granítico Lavras e vulcânicas associadas, RS. Braz. J. Geol. 18, 369–375.

Paim, P.S.G., Chemale Jr., F., Lopes, R.C., 2000. A Bacia do Camaquã. In: Holz, M., De Ros, L.F. (Eds.), Geologia do Rio Grande do Sul, Ed Da Universidade/UFRGS, Porto Alegre, pp. 231–374.

Pearce, J., 1996. Sources and settings of granitic rocks. Episodes 19, 120–125.

Porcher, C.A., Lopes, R. da C., 2000. Cachoeira do Sul, folha SH.22–Y–A, escala 1: 250.000, estado do Rio Grande do Sul: Programa de Levantamentos Geológicos Básicos do Brasil. CPRM, Rio de Janeiro, CD ROM.

Reed, M.H., Palandri, J., 2006. Sulfide mineral precipitation from hydrothermal fluids, in: Vaughan, D.J. (ed.), sulfide mineralogy and geochemistry. Rev. Mineral. Geochem. 61 (1), 609–631.

Reischl, J.L., 1978. Mineralizações cupríferas associadas a vulcânicas na Mina do Seival. Anais do XXX Congresso Brasileiro de Geologia, Recife, pp. 1568–1582.

Remus, M.V.D., Hartmann, L.A., McNaughton, N.J., Groves, D.I., Reischl, J.L., 2000. A distal magmatic–hydrotermal origin for the Camaquã Cu (Au–Ag) and Santa Maria Pb, Zn (Cu–Ag) deposits, southern Brazil. Gondwana Res. 3, 155–174.

Remus, M.V.D., McNaughton, N.J., Hartmann, L.A., Groves, D.I., 1997. Pb and S Isotope Signature of Sulfides and Constraints on Timing and Sources of Cu (Au) Mineralization at the Camaquã and Santa Maria Mines, Caçapava do Sul, Southern Brazil. South American Symposium Isotopic Geology (SSAGI), São Paulo, pp. 253–255.

Renac, C., Mexias, A.S., Gomes, M.E.B., Ronchi, L.H., Nardi, L.V.S., Laux, J.H., 2014. Isotopic fluid changes in a Neoproterozoic porphyry epithermal system: the Uruguay mine, southern Brazil. Ore Geol. Rev. 60, 146–160.

Reynolds, R.C., 1985. NEWMOD, a Computer Program for the Calculation of One-dimensional Diffraction Patterns of Mixed-layered Clays. R C Reynolds, 8 Brook Rd., Hanover, NH, USA.

Ribeiro, M., Fantinel, L.M., 1978. Associacões petrotectônicas do Escudo Sul–Riograndense: I Tabulação e distribuicão das associações petrotectônicas do Escudo do Rio Grande do Sul. Inheringia Serviço Geológico 5, 19–54.

Robertson, J.F., 1966. Revision of the stratigraphy and nomenclature of rock units in the Caçapava–Lavras region – State of Rio Grande do Sul, Brazil. Notas e Estudos 1, 41–54.

Robertson, J.F., Johnson, R.F., 1966. Copper Deposits of the Caçapava do Sul – Lavras do Sul Region, State of Rio Grande do Sul (Technical Letter – Brazil Investigations).

Saalmann, K., Gerdes, A., Lahaye, Y., Hartmann, L.A., Remus, M.V.D., 2011. A multiple accretion at the eastern margin of the Rio de la Plata craton: the prolonged Brasiliano orogeny in southernmost Brazil. Int. J. Earth Sci. 100, 355–378.

Saalmann, K., Hartmann, L.A., Remus, M.V.D., 2007. The assembly of west Gondwana—the view from the Rio de la Plata craton. In: Linnemann, U., Nance, R.D., Kraft, P., Zulauf, G. (Eds.), The Evolution of the Rheic Ocean: From Avalonian–Cadomian Active Margin to Alleghenian–Variscan Collision. Geological Society of America Special Paper Vol. 423, pp. 1–26.

Saalmann, K., Hartmann, L.A., Remus, M.V.D., Koester, E., Conceição, R.V., 2005. Sm–Nd isotope geochemistry of metamorphic volcanosedimentary successions in the São Gabriel Block, southernmost Brazil: evidence for the existence of juvenile Neoproterozoic oceanic crust to the east of the Rio de la Plata craton. Precambrian Res. 136, 159–175.

Schleicher, A.M., Hofmann, H., van der Pluijm, B.A., 2013. Constraining clay hydration state and its role in active fault systems. Geochem. Geophys. Geosyst. 14, 1039–1052.

Sommer, C.A., Lima, E.F., Nardi, L.V.S., Liz, J.D., Waichel, B.L., 2006. The evolution of Neoproterozoic magmatism in southernmost Brazil: shoshonitic, high-K tholeiitic and silica–saturated, sodic, alkaline volcanism in post-collisional basins. An. Acad. Bras. Cienc. 78, 573–589.

Teixeira, E.A., 1937. Cobre no Estado do Rio Grande do Sul. Div. Fom. Prod. Min. – Bol. 22 (RJ).

Vidal, O., Baldeyrou, A., Beaufort, D., Fritz, B., Geoffroy, N., Lanson, B., 2012. Experimental study of the stability and phase relations of clays at high temperature in a thermal gradient. Clay Clay Miner. 60, 200–255.

Vieira Jr., N., Soliani Jr., E., 1989. Um Novo Modelo Genético–Evolutivo para o Maciço Granítico de Lavras do Sul, RS. Acta Geológica Leopoldensia 12, 143–160.

Vogels, R.J.M.J., Kerldaoffs, M.J.H.V., Geus, J.W., 1995. Non-hydrothermal synthesis, characterisation and catalytic properties of saponite clays. Stud. Surf. Sci. Catal. 91, 1153–1161.

Wernick, E., 1978. Contribuição à estratigrafia do Pré-cambriano do leste do estado de São Paulo e áreas vizinhas. Braz. J. Geol. 8, 206–216.

Wildner, W., Lima, E.F., Nardi, L.V.S., Somer, C.A., 2002. Volcanic cycles and setting in the Neoproterozoic III to Ordovician Camaquã Basin succession in southern Brazil: characteristic of post-collisional magmatism. J. Volcanol. Geotherm. Res. 118, 261–283.

Wildner, W., Ramgrab, G.E., Lopes, R.C., Iglesias, C.M.F., 2008. Geologia e Recursos Minerais do Rio grande do Sul. Escala 1 750000. Brasil, Porto Alegre, CD ROM, CPRM – Serviço geológico do.

Wildner, W., Nardi, L.V.S., Lima, E.F., 1999. Post-collisional alkaline magmatism on the Taquarembó plateau: a well preserved Neoproterozoic–Cambrian Plutono–volcanic association in southern Brazil. Int. Geol. Rev. 41, 1082–1098.